Post-combustion CO2 capture by coupling [emim] cation based ionic liquids with a membrane contactor; Pseudo-steady-state approach

Qazi Sohaib, Jose Manuel Vadillo, Lucía Gómez-Coma, Jonathan Albo, Stéphanie Druon-Bocquet, Angel Irabien, José Sanchez-Marcano

Post-Combustion CO_2 Capture by Coupling [emim] Cation Based Ionic Liquids with a Membrane Contactor; Pseudo-Steady-State Approach

Qazi Sohaib[1], Jose Manuel Vadillo[2], Lucía Gómez-Coma[2], Jonathan Albo[2], Stéphanie Druon-Bocquet[1], Angel Irabien[2], José Sanchez-Marcano[1]

1 : Institut Européen des Membranes, IEM – UMR 5635, CNRS, ENSCM, Université de Montpellier, Montpellier, France.

2 : Chemical and Biomolecular Engineering Department, Universidad de Cantabria, Av. Los Castros, 39005 Santander, Spain.

Abstract

This study demonstrates the coupling of Ionic liquids (ILs) with a membrane contactor for post-combustion CO_2 capture at moderate pressures and temperatures. ILs 1-ethyl-3-methylimidazolium methyl sulfate([emim][$MeSO_4$]), 1-ethyl-3-methylimidazolium dicyanamide([emim][DCA]), 1-ethyl-3-methylimidazolium ethyl sulfate([emim][$EtSO_4$]) and 1-ethyl-3-methylimidazolium acetate ([emim][AC]) were selected due to their high thermal stability, moderate viscosity and surface tension, as well as high CO_2 solubility. No wetting conditions were confirmed for the polypropylene membrane by measuring contact angle, liquid entry pressure (LEP) and SEM of fiber surface before and after the operation. ILs were recirculated in the setup until reaching pseudo-steady-state. All four ILs were able to capture a substantial amount of CO_2 during the specified operation time. Initially, very high values of CO_2 mass transfer flux and experimental overall mass transfer coefficient were obtained which further decreased with operation time and reached a nearly constant value at pseudo-steady-state. Effect of CO_2 loading of the ILs and temperature on enhancement factor and first order rate constant were evaluated. The absorption behavior and kinetics were strongly influenced by the CO_2 concentration in the ILs, which divides the absorption process in two steps; an initial faster absorption at the gas-liquid interface and later slower absorption in the bulk of the IL. Finally, a pseudo-steady-state modelling approach was implemented and validated.

Keywords: Post-Combustion CO_2 Capture, pseudo-steady-state, Membrane Contactor, Ionic Liquid, Absorption Kinetics

Nomenclature

A	Area (m^2)
C	Concentration $(mol\ m^{-3})$
d	diameter (m)
D	Diffusivity $(cm^2\ s^{-1})$
E	Enhancement factor (-)
H_{px}	Inverse Henry's law constant (MPa)
H_d	Dimensionless Henry's law constant (-)
j	Molar Flux $(mol\ m^{-2}\ s^{-1})$
K_r	Rate constant (s^{-1})
K	Mass transfer coefficient $(m\ s^{-1})$
L	Length of membrane(m)
M	Molar weight $(kg\ mol^{-1})$
ñ	Number of moles
N	Number of fibers
P	Pressure (Pa)
Q	Volumetric flowrate $(m^3\ s^{-1})$
ŕ	Reaction rate $(mol\ m^{-3}\ s^{-1})$
Ŕ	Perfect gas constant $(m^3\ Pa\ mol^{-1}.K^{-1})$
r	Radius (m)
R_e	Reynolds number (-)
S_c	Schmidt number (-)
S_h	Sherwood number (-)
t	Time(s)
T	Temperature (K)
U	Interstitial velocity $(m\ s^{-1})$
v	Molar volume $(cm^3.mol^{-1})$
V	Volume (m^3)
x^*	Mole fraction of CO_2 in IL (-)
y^*	Mole fraction of CO_2 in gas (-)

Subscripts

CO_2	Carbon dioxide
g	Gas
l	Liquid
m	membrane
in	Inlet
out	Outlet
i	Inner
o	Outer
h	Hydraulic
IL	Ionic Liquid
lm	Log mean
r	Radial coordinate
z	Axial coordinate

Greek symbols

μ	Viscosity (cP)
Ø	Packing fraction of Contactor (-)
ρ	Density $(g\ cm^{-3})$
ε	Membrane porosity (-)
$\mathcal{T}$	Residence time (s)
τ	Membrane tortuosity (-)
δ	Membrane thickness (m)
ϒ	Surface tension $(mN\ m^{-1})$
α	CO_2 loading $(mol\ mol^{-1})$

1 Introduction

CO_2 is believed to be the largest contributor (~80%) to all greenhouse gases (Hajilary and Rezakazemi, 2018; Rezakazemi et al., 2019); causing higher earth surface temperature, global warming and other severe climatic disturbances. Human activities have caused an increase of 100 ppm (36%) in atmospheric CO_2 concentration over the past 250 years (Barker, 2007; Jie et al., 2013). CO_2 capture (CC) is one of the most promising options to minimize the influence of fossil fuel utilization on climate change (Rezakazemi et al., 2018; Yang et al., 2008). Post-combustion carbon capture (PCC), pre-combustion carbon capture and oxyfuel-combustion carbon capture are the three widely used technologies, among which PCC is the most promising one as it can be retrofitted to existing units in power plants (Dai and Deng, 2016; Sohaib et al., 2020; Zhao et al., 2016). PCC based on liquid absorbents is known as state-of-the-art CC technology with high CO_2 removal efficiency (> 80%) even at low pressure and CO_2 concentrations (Figueroa et al., 2008). Although industrial scale and other conventional absorbers used for PCC based on liquid absorbents are relatively efficient, it still faces some serious problems like substantial energy consumption, corrosion, solvent loss by entrainment, flooding and foaming. Membrane contactor technology is a promising alternative to overcome these problems (Gabelman and Hwang, 1999).

Membrane contactor absorption is a hybrid technology combining the advantages of absorption and membrane contactor (Dai and Deng, 2016; Zhang et al., 2013). Advantages of membrane contactors over other conventional absorbers and packed columns include large and constant interfacial area, no flooding, foaming and entrainment, flexible operability on gas and liquid sides, modularity and linear scaling (Gabelman and Hwang, 1999; Li and Chen, 2005; Qazi et al., 2020a; Razavi et al., 2016). Falk-Pedersen et al. (2005) used a membrane contactor for absorption of exhaust gas from gas turbine, which significantly eliminated or reduced many operating problems. Other major benefits reported were a reduction of footprint requirements up to 50%, savings of operating cost up to 52% and a capital cost reduction of 40%. The major disadvantage of membrane contactor is an increased mass transfer resistance due to the membrane itself or membrane pore wetting which can significantly increase the mass transfer resistance leading to a sharp drop in absorption performance (Mosadegh-Sedghi et al., 2014; Rangwala, 1996). Membrane pore wetting can be prevented by maintaining the pressure below liquid entry pressure (LEP) also called breakthrough pressure. According to Laplace-young equation, LEP can be increased by increasing cosine of the contact angle, using absorbents of high surface tension and smaller membrane pores. Li and Chen, (2005) and Mosadegh-Sedghi et al. (2014) also suggested the above mentioned parameters to control pore wetting with the addition of using hydrophobic membranes, employing non-corrosive and membrane compatible absorbents and maintaining transmembrane pressure lower than LEP. The porous membranes used in membrane contactors are usually made of hydrophobic material such as polypropylene (PP), polyethylene (PE), polytetrafluoroethylene (PTFE) and polyvinylidenefluoride (PVDF). These membranes are mostly reported to be used for CO_2 capture due to their high hydrophobicity and good stability (Chabanon et al., 2015; Dai et al., 2016a). Selection of absorbents for CC in membrane contactors is very critical because of the various problems caused by conventional absorbents (Constantinou et al., 2014; Dindore et al., 2004). Amine based solvents have been mostly used so far, because of their large cyclic capacities. However, use of these solvents is threatened by their high volatility, large amount of solvent loss, degradation at high temperature and high corrosion rate (Iliuta et al., 2015; Wang et al., 2013). Another approach to overcome these problems is the use of Ionic liquids (ILs) in combination with membrane contactors (Qazi et al., 2020b).

ILs are organic salts having extraordinarily high CO_2 solubility, negligible vapor pressure and high thermal stability (Li et al., 2016), which leads to almost zero solvent loss and lower energy consumption during regenerations (Ramdin et al., 2012). Another advantage of ILs are their low toxicity and relatively low corrosiveness, which are almost two magnitudes lower than commonly used amines (Papatryfon et al., 2014). ILs are classified in two categories, room temperature ILs (RTILs) and Task Specific Ionic Liquids. RTILs are considered to behave as typical physical solvents for CO_2 and other gases. Gas solubility in RTILS are widely represented by Henry's law constant (Dai et al., 2016b; Lei et al., 2014). Imidazolium based ILs are widely reported to be used for CO_2 capture. Studies have reported less effect of alkyl chain cations on CO_2 solubility compared to anions which has strong influence on the solubility of CO_2 (Chen et al., 2006; Zhang et al., 2012). Solubility and Henry's Law constant of CO_2 in various RTILs have been extensively studied and reported in the literature (Blath et al., 2012, 2011; Mejía et al., 2013; Ramdin et al., 2012; Soriano et al., 2009; Yim et al., 2018; Yokozeki et al., 2008).

In the past few years, many researchers have applied ILs in combination with membrane contactors for gas separation. For example Dai and Deng, (2016) used IL 1-Butyl-3-methlyimidazolium tricyanomethanide ([Bmim][TCM]) for CO_2 absorption in microfiltration glass membrane. Study has reported a decrease in CO_2 flux from 3.09 10^{-5} mol m^{-2} s^{-1} to 2.13 10^{-5} mol m^{-2} s^{-1} by an increase from temperature to 353.15 K. A decrease of 22 % in overall mas transfer coefficient was reported due to only 1 % pore wetting. In another study the author used the same IL [Bmim][TCM] to study and compare the compatibility of six different polymeric membranes for CO_2 absorption (Dai et al., 2016a). A composite membrane of material Teflon-PP was observed to be more stable. Higher CO_2 flux was observed for all types of membranes at high gas flow rates. Lu et al. (2013), (2014), (2015) and (2017), developed membrane absorption and vacuum regeneration unit for absorption and regeneration/stripping of CO_2 with ILs 1-butyl-3-methyl-imidazolium tetrafluoroborate ([bmim][BF_4]), 1-(3-aminopropyl)-3-methyl-imidazolium tetrafluoroborate ([apmim][BF_4]), monoethanolamine glycinate ([MEA][GLY]) and mixture of 2-amino-2-methyl-1-propanol (AMP) with [bmim][BF_4] and [apmim][BF_4]. IL [apmim][BF_4], as a chemical absorbent was able to achieve a higher membrane flux of 6.86 10^{-4} mol m^{-2} s^{-1} compared to a physical absorbent [bmim][BF_4], having a membrane flux of 2.12 10^{-5} mol m^{-2} s^{-1}. IL [bmim][BF_4] was very easy to regenerate, even at low temperature and vacuum degrees. IL [MEA][GLY], which is a protic amino acid functionalized IL could reach a membrane flux of 3.25 10^{-4} mol m^{-2} s^{-1}. Mixture of [apmim][BF_4] and AMP achieved a very high membrane flux of 1.05 × 10^{-3} mol m^{-2} s^{-1}. Gómez-Coma et al. (2014) and Albo et al. (2010) used IL 1-ethyl-3-methylimidazolium ethyl sulfate in their studies for CO_2 absorption in membrane contactor. An overall mass transfer coefficient of 0.7 10^{-6} m s^{-1} and enhancemnt factor of 1.2 was observed. Chau et al. (2016) and (2014) used 1-Butyl-3-methylimidazolium dicyanamide ([Bmim][DCA]) for pressure swing membrane absorption process to absorb CO_2 from low temperature shifted syngas. An increase in temperature from 298 K to 348 K has resulted a decrease in % CO_2 (in CO_2 product stream) from 89.9 % to 79.4 %. Increasing pressure from 100 psig to 250 psig resulted an increase in % CO_2 from 89.9 % to 92.9 %.

This work aims to develop a pseudo-steady-state membrane contactor absorption process for CO_2 absorption with four different imidazolium based ILs, 1-ethyl-3-methylimidazolium methyl sulfate ([emim][$MeSO_4$]), 1-ethyl-3-methylimidazolium dicyanamide ([emim][DCA]), 1-ethyl-3-methylimidazolium ethyl sulfate ([emim][$EtSO_4$]) and 1-ethyl-3-methylimidazolium acetate ([emim][AC]). To our knowledge it is the first time that ILs [emim][$MeSO_4$] and [emim][DCA] have been tested for CO_2 absorption in a membrane contactor. A mesoporous hydrophobic polypropylene (PP) membrane

contactor was selected for current absorption process. ILs were allowed to flow through shell side in a closed loop to develop a pseudo-steady-state and to extensively study the variations in mass transfer kinetics and absorption behavior of ILs with increase in CO_2 concentration in ILs. None of the detailed investigations of these phenomena have been performed previously. ILs [emim][$MeSO_4$] (Santos and Baldelli, 2009; Sumon and Henni, 2011; Yim et al., 2018), [emim][DCA] (Almeida et al., 2012; Huang and Peng, 2017; Quijada-Maldonado et al., 2012), [emim][$EtSO_4$] (Carvalho et al., 2014; Fröba et al., 2008; Jalili et al., 2010; Quijada-Maldonado et al., 2012; Soriano et al., 2009) and [emim][Ac](Almeida et al., 2012; Quijada-Maldonado et al., 2012; Yim et al., 2018; Yokozeki et al., 2008) have been reported as excellent absorbents with high solubility for CO_2 and moderate surface tensions which makes them very feasible to be used for CO_2 absorption operation with hydrophobic membranes. Both ILs and PP fibers were characterized based on various techniques. LEP was calculated from surface tension and contact angle measurements to ensure no-wetting conditions. The setup was tested against various operating conditions. Variations of mass transfer kinetics with increase in CO_2 concentration in four [emim] cation based ILs were systematically studied in terms of CO_2 outlet concentration, experimental overall mass transfer coefficient, logarithmic means of the driving force, shell side mass transfer coefficient and mass transfer enhancement factor.

2 Experimental

2.1 Materials

ILs ([emim][$MeSO_4$], ([emim][DCA]), ([emim][$EtSO_4$]) and ([emim][AC]) with more than 95 % purity were purchased from Sigma-Aldrich. Carbon dioxide (99.7 % ±0.01 vol%) and Nitrogen (99.9 % ±0.001 vol%) were purchased from Air Liquide, Spain. A membrane contactor (1 x 5.5 MiniModule™) with hydrophobic hollow fibers was supplied by Liqui-Cel ™, USA. The modules consist of mesoporous polypropylene hollow fibers with 40 % porosity and mean pore diameter of 0.04 µm, potted with polyurethane. The detailed specifications of the membrane contactor are presented in Table 1.

Table 1 Specifications of the membrane module

Parameter	Value	unit
Membrane material	Polypropylene	-
Inner diameter of the tube (d_i)	$2.2\ 10^{-4}$	m
Outer diameter of the tube (d_o)	$3.0\ 10^{-4}$	m
Membrane thickness (δ)	$0.4\ 10^{-4}$	m
Inner diameter of the module (d_c)	$2.1\ 10^{-2}$	m
Length of the contactor (L)	0.115	m
Number of fibers (N)	2300	-
Membrane pore diameter(d_p)	0.04	µm
Effective inner membrane area (A)	0.18	m^2
Lumen side volume (V_g)	$1.6\ 10^{-5}$	m^3
Shell side volume (V_l)	$2.5\ 10^{-5}$	m^3
Porosity (ε)	40	%
Packing factor (Ø)	0.39	-
Tortuosity (τ)[a]	6.4	-

[a] $\tau = \frac{(2-\varepsilon)^2}{\varepsilon}$ (Iversen et al., 1997)

2.2 Materials characterization

ILs used in this work were characterized by measuring surface tension and contact angle. Surface tension was measured with a Langmuir device (KSV NIMA Langmuir-Blodgett) using a Wilhelmy plate made of platinum partially immersed in the IL. The apparatus determines the force (gravity, surface tension and buoyancy) on the plate due to surface tension. The contact angle of the ILs on membrane surface was measured by a contact angle meter (DIGIDROP-Modular contact angle technology, GBX). The instrument is able to measure contact angle with $\pm 0.1^{o}$ of accuracy with maximum frame recording speed of 50/60 images/s. The associated software automatically controls the droplet volumes and its deposition on the surface. The software provides various polynomial and manual techniques to measure the average contact angle. Other characteristics of ILs as density, viscosity and CO_2 solubility were calculated with correlations or taken from the literature.

The possible morphological changes of the membrane surface and its porous structure due to long term contact with ILs were investigated with scanning electron microscope (Hitachi S-4800 FE-SEM). Prior to SEM analysis, samples were sputter coated with platinum for 5 minutes to ensure better conductivity. Samples were observed at an acceleration voltage of 2kv.

2.3 Experimental setup

A membrane contactor setup coupled with ILs, suitable for post-combustion applications, was applied in this current study. The setup is illustrated in Figure 1. The feed gas mixture containing 15 % CO_2 and N_2 (rest to balance) was introduced through the lumen side of the fibers. The gas mixture was kept in open loop conditions, i.e CO_2 concentration at the gas side inlet was always kept constant (15 % by Vol). Gas mass flowmeters (Alicat scientific, MC–gas mass flow controller, Spain) were used to measure and control the flow of gases inside the fibers. The gas side pressure was nearly kept at atmospheric level. Operating conditions of the absorption process are presented in Table 2. The CO_2 concentration at the inlet and outlet of the membrane contactor was analyzed by a CO_2 analyzer (Geotech, G110 0-100%, UK). IL was kept in a reservoir, from where it was pumped through the shell side using a digital gear pump (Cole-Parmer Gear Pump System, Benchtop Digital Drive, 0.017 mL/rev, 220 VAC, Spain) to maintain a constant flowrate and avoid fluctuations. The IL was recirculated from the reservoir in a closed-loop. Liquid side pressure was always kept higher (but very far from LEP to avoid wetting) than the gas side to avoid penetration of the gas into the liquid side. Experimental setup was kept inside an oven and all experiments were carried out in controlled temperature environment to maintain isothermal conditions. ILs and gas stream were introduced to the module counter currently. During recirculation, IL absorbs CO_2 on the gas liquid interface which accumulates on the shell side. CO_2 concentration at the outlet gas stream was continuously monitored by CO_2 analyzer. IL was recirculated for CO_2 absorption until it reaches pseudo-steady-state. After reaching pseudo-steady-state the CO_2 desorption/stripping was initiated using an N_2 sweep at various temperature levels. IL was recirculated similarly in a closed-loop. The CO_2 desorbing from IL on the interface diffused inside the pores of membrane filled with N_2, whose concentration was continuously analyzed at the gas side outlet.

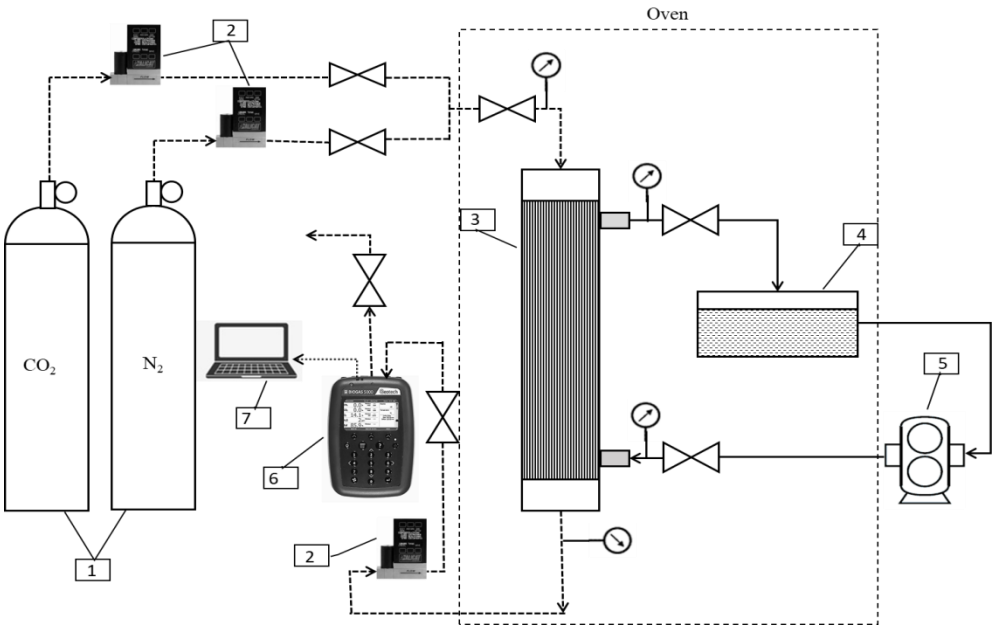

Figure 1. Schematic representation of the experimental setup; 1-CO_2 and N_2 gas cylinders, 2-Gas flowmeters, 3-membrane module, 4-Ionic liquid Reservoir, 5-Gear Pump, 6-CO_2 analyzer, 7-Computer connected to CO_2 analyzer

Table 2 Operating conditions

Parameter/Property	Value	Unit
Ionic liquids	[emim] [$MeSO_4$] ≥ 95%	-
	[emim] [DCA] ≥ 95%	-
	[emim] [$EtSO_4$] ≥ 95%	-
	[emim] [AC] ≥ 95%	-
CO_2 concentration	15	Vol %
T	288-323	K
Q_g	20-200	ml min^{-1}
Q_{IL}	60	ml min^{-1}
$P_{g\text{-}in}$	1.03	Bar
$P_{l\text{-}in}$	2.40	Bar

3 Theory

3.1 Mass transfer kinetics

The overall gas mass transfer in membrane contactor encounters three main resistances i.e. resistance in the gas phase, membrane and liquid phase. Resistance in series approach can be used to combine these individual resistances.

$$R_{ov} = R_g + R_m + R_l \quad (1)$$

A hollow fiber membrane contactor is used with gas on the lumen side and liquid on the shell side. The gas liquid interface is located on the outer boundary of the tubes assuming no wetting conditions. Considering an enhancement factor (E) for chemical reaction on the shell side, the equation can be written as below(Ortiz et al., 2010).

$$\frac{1}{K_{ov}} = \frac{d_o}{k_g d_i} + \frac{d_o}{k_m d_{lm}} + \frac{1}{k_l H_d E} \quad (2)$$

In the above equation, $k_g(m\ s^{-1})$, $k_m(m\ s^{-1})$ and $k_l(m\ s^{-1})$ are individual mass transfer coefficients of gas, membrane and liquid phase while d_o, d_i and d_{lm} are the outer, inner and log mean diameters of the membrane fiber. H_d in the above equation represents dimensionless Henry's law constant. This parameter is very important as it represents CO_2 solubility in ILs and is mostly used for RTILs (Lei et al., 2014; Wang et al., 2011). Henry's law constant can be calculated by the following equation (Luis et al., 2009; Sander, 2015).

$$H_d = \frac{C_g^*}{C_l^*} = \frac{y^*}{x^*}\frac{\rho_g}{\rho_l} = \frac{y^*}{x^* \rho_l}\frac{P_T}{RT} \quad (3)$$

Where y^* and x^* represents equilibrium mole fractions of CO_2 in gas and liquid phase at certain pressure and temperature, while ρ_l represents molar density ($mol\ L^{-1}$) of the liquid. Experimental PTx data (equilibrium mole fractions of CO_2 between gas and liquid phase) for ILs [emim][$MeSO_4$], [emim][DCA], [emim][$EtSO_4$] and [emim][Ac] are available from the literature (Carvalho et al., 2014; Huang and Peng, 2017; Jalili et al., 2010; Mejía et al., 2013; Soriano et al., 2009; Yim et al., 2018; Yokozeki et al., 2008). As reported previously, contributions of the gas and membrane phase can be neglected, by considering non-wetting conditions and gas filled membrane pores (Ortiz et al., 2010). Equation 2 can then be rewritten as below.

$$\frac{1}{K_{ov}} = \frac{1}{k_l H_d E} \quad (4)$$

Several empirical correlations have been proposed by different authors for shell side liquid mass transfer coefficient in parallel flow membrane contactor, depending upon the operating conditions of the liquid flowing and characteristics of the membrane contactor. The correlation developed by Li et al. has been used in this study as it closely meets the conditions of current absorption process (Shen et al., 2010).

$$Sh_s = \left(\frac{k_l d_h}{D_l}\right) = (0.52 - 0.64\emptyset) R_e^{(0.36+0.3\emptyset)} S_c^{0.33};\ 0 < R_e < 100;\ 0.30 < \emptyset < 0.70 \quad (5)$$

While d_h, D_l, $\emptyset$, R_e and S_c are hydraulic diameter, CO_2 diffusivity in liquid phase, packing fraction of membrane contactor, Reynolds number and Schmidt number, respectively. These parameters are calculated as under.

$$d_h = \frac{d_{c-i}^2 - N d_o^2}{d_{c-i} \mp N d_o} \quad (6)$$

While d_{c-i}, d_o and N represent contactor inner diameter, fiber outer diameter and number of fibers, respectively. CO_2 diffusivity in liquid phase was predicted by the correlation developed by Morgan et al. (2005).

$$D_l = 2.66 \,.\, 10^{-3} \frac{1}{\mu_{IL}^{0.66} v_{CO_2}^{1.04}} \quad (7)$$

Where $\mu_{IL}(cP)$ and $v_{CO_2}(cm^3.mol^{-1})$ are viscosity of IL and molar volume of CO_2. The correlation developed by Morgan et al. is very well known for CO_2 diffusivities in imidazolium cation based ILs with different anions and has been confirmed experimentally by many authors (Moganty and Baltus, 2010; Zubeir et al., 2015). Reynolds number is calculated as follows.

$$R_e = \frac{4\rho_{IL}Q}{\pi\mu_{IL}(d_{c-i}+Nd_0)} \quad (8)$$

The CO_2 mass transfer flux can be calculated from the following equation.

$$j_{CO_2-g} = \frac{1}{A}\left(\frac{d\tilde{n}}{dt}\right) = \frac{Q_{g-in}\,C_{g-in} - Q_{g-out}C_{g-out}}{A} = K_{exp}\,\Delta C_{g-lm} \quad (9)$$

Where ñ represents moles of CO_2, Q_{g-in} and Q_{g-out} are gas side inlet and outlet flow rates($m^3.s^{-1}$), respectively, C_{g-in} and C_{g-out} are gas side inlet and outlet concentrations($mol.m^{-3}$) of CO_2, respectively, while K_{exp} denotes the experimental overall mass transfer coefficient ($m\ s^{-1}$). K_{exp} can be calculated from mass transfer flux and concentration gradient. ΔC_{g-lm} in the above equation represents logarithmic mean of the driving force which can be calculated using the equation below.

$$\Delta C_{g-lm} = \frac{\left(C_{g-in}-C^*_{g-in}\right)-\left(C_{g-out}-C^*_{g-out}\right)}{\ln\left(\frac{C_{g-in}-C^*_{g-in}}{C_{g-out}-C^*_{g-out}}\right)} \quad (10)$$

Where C^*_{g-in} and C^*_{g-out} represents equilibrium concentration of the gas phase with corresponding CO_2 concentration in the liquid phase C^*_l. Equilibrium concentration of gas phase C^*_g can be found using equation 3 ($C^*_g = H_d\ C^*_l$) based on Henry's Law constant. The enhancement factor E determines the absorption rate of CO_2 in absorbents and quantifies how and up to what extent the absorption is enhanced by the chemical reaction (Dindore and Versteeg, 2005; Lu et al., 2005). Experimental overall mass transfer coefficient, K_{exp} calculated from equation 9 can be used instead of K_{ov} in equation 4 to predict the enhancement factor for CO_2 absorption in ILs. Equation 4 after rearranging can be written as:

$$E = \frac{K_{exp}}{k_l H_d} \quad (11)$$

Considering first order interfacial chemical reaction, mass transfer rate for gas absorption in membrane contactor can be described as;

$$-\acute{r}_{CO_2} = \left(-\frac{dC_{CO_2}}{dt}\right)_g = \frac{1}{V_g}\left(-\frac{d\tilde{n}}{dt}\right) = K_r\,\Delta C_{g-lm} \quad (12)$$

V_g in the above equation represents gas side volume. The equation represents the mechanism of first order chemical reaction of CO_2 with IL. Combining equation 9 and 12 can give us the following new equation.

$$j_{CO_2-g}\,A = \acute{r}_{CO_2}\,V_g \quad (13)$$

By combining equation 12 and 13 we can get the following equation.

$$j_{CO_2-g} = \acute{r}_{CO_2}\left(\frac{V_g}{A}\right) = K_r\left(\frac{V_g}{A}\right)\Delta C_{g-lm} \quad (14)$$

The final equation for the surface reaction rate (K_r) of CO_2 with IL is expressed as;

$$K_r = K_{exp}\left(\frac{A}{V_g}\right) \quad (15)$$

The kinetic constant K_r (s^{-1}) represents first order gas liquid reaction, which will be used to quantify the chemical absorption potential of ILs and its variation with increase of CO_2 concentration in ILs as it is directly proportional to experimental overall mass transfer coefficient.

3.2 Modeling approaches

A two-dimensional (2D) modelling approach was used to develop a dynamic model for the pseudo-steady-state process explained in section 2.3. Membrane characteristics and operating conditions for the model were adopted from Tables 1 and 2 of the experimental section. The process was based on pseudo-steady-state conditions in which IL was recirculated in a closed loop while gas could flow in an open loop. The following hydrodynamic and thermodynamic assumptions were taken for the development of the model:

a) Pseudo-steady-state (IL in closed loop while gas in open loop) and isothermal conditions
b) Countercurrent mode for gas and IL flow in membrane contactor
c) Laminar flow with Fully developed velocity profile in the shell and tube
d) Ideal gas behavior
e) Application of Henry's law on gas-liquid interface for CO_2 with neglected solubility of N_2
f) Non-wetted membrane (unless mentioned) with no selectivity
g) Membrane mass transfer using Fick's diffusion through porous media and neglecting convective contributions
h) Contributions of advection and diffusion to mass balance solved by considering local concentrations
i) Perfectly stirred absorbent tank

3.2.1 Model equations

Mass and momentum differential balance based on the above-mentioned assumptions for hydrodynamics and thermodynamics are presented below.

$$\frac{\partial C_i}{\partial t} = -\nabla . C_i U - \nabla . j_i \tag{16}$$

In the above equation $\mathrm{C_i (mol.\,m^{-3})}$, $\mathrm{U\ (ms^{-1})}$ and $\mathrm{j_i\ (mol.\,m^{-2}.\,s^{-1})}$ represents concentration of the solute, velocity and mass transfer flux, respectively. For the gas (equation 17), membrane (equation 18) and liquid (equation 19), the above equation is written as below.

$$\frac{\partial C_g}{\partial t} + D_g \left[\frac{\partial^2 C_g}{\partial r^2} + \frac{1}{r}\frac{\partial C_g}{\partial r} + \frac{\partial^2 C_g}{\partial z^2}\right] = U_{z,g}\frac{\partial C_g}{\partial z} \tag{17}$$

$$\frac{\partial C_m}{\partial t} + D_m \left[\frac{\partial^2 C_m}{\partial r^2} + \frac{1}{r}\frac{\partial C_m}{\partial r} + \frac{\partial^2 C_m}{\partial z^2}\right] = 0 \tag{18}$$

$$\frac{\partial C_l}{\partial t} + D_l \left[\frac{\partial^2 C_l}{\partial r^2} + \frac{1}{r}\frac{\partial C_l}{\partial r} + \frac{\partial^2 C_l}{\partial z^2}\right] = U_{z,l}\frac{\partial C_l}{\partial z} \tag{19}$$

For the fluid in the lumen side Hagen-Poiseuille equation with no slip conditions leads to a fully developed velocity profile, while for the velocity in shell side Happel's free surface model was used (Happel, 1959).

$$U_{z,g} = 2u_g \left[1 - \left(\frac{r}{r_1}\right)^2\right] \tag{20}$$

$$U_{z,l} = 2u_l\left[1-(\frac{r_2}{r_3})^2\right]\frac{(r/r_3)^2-(r_2/r_3)^2+2\ln(r_2/r)}{3+(r_2/r_3)^4-4(r_2/r_3)^2+4ln(r_2/r_3)}, \quad r_3 = r_2\sqrt{\frac{1}{1-\emptyset}}, \quad 1-\emptyset = \frac{Nr_2^2}{r_{c-i}{}^2} \tag{21}$$

Diffusivity of CO_2 in the gas (D_g) and ionic liquid (D_l) are measured by correlations developed by Fuller et al. (1966) and Morgan et al. (2005), respectively. The later diffusivity correlation is presented in the preceding section as of equation 7. While for the membrane (D_m), combined effects of gas diffusivity, D_g and Knudsen diffusivity D_{Kn} were considered (details in supplementary data).

$$D_g = \frac{0.01013.T^{1.75}\left(\frac{1}{M_{CO_2}}+\frac{1}{M_{N_2}}\right)^{0,5}}{P\left[\left(\sum \upsilon_{CO_2}\right)^{\frac{1}{3}}+\left(\sum \upsilon_{N_2}\right)^{\frac{1}{3}}\right]^2} \tag{22}$$

Details of the temperature dependency of the viscosity are presented in supplementary data section 1.1.

The continuous evolution of ILs concentration in the reservoir was measured by applying a transient state differential equation across the reservoir.

$$Q_{IL}\left(C_{r,in}(t)-C_{r,out}(t)\right) = V_{IL}\frac{dC_{r(t)}}{dt} \tag{23}$$

Where C_r represents the concentration of CO_2 in the IL reservoir. The equation can be further written in the final form as;

$$C_{r,out}(t+\Delta t) = \frac{\Delta t}{\mathcal{T}_{IL}}C_{r,in}(t) + C_r(t)\left[1+\frac{\Delta t}{\mathcal{T}_{IL}}\right]; C_{r,in}(t) = \frac{\int\int_{r=r_2}^{r=r_3} C_l(r)rdrd\theta}{\int\int_{r=r_2}^{r=r_3} rdrd\theta}; \text{at } t=0,\ C_{r,in}=0;$$

$$\mathcal{T}_{IL} = \frac{V_{IL}}{Q_{IL}} \tag{24}$$

The term $C_{r,out}(t+\Delta t)$ corresponds to the outlet concentration of the reservoir at time $t+\Delta t$, which is input to the shell side of the contactor. Coupling the above-mentioned equation develops a pseudo-steady-state for which the boundary conditions (BCs) are presented below.

3.2.2 Boundary conditions

BCs for the mass balance equations of the three domains and IL reservoir are presented in Table 3 below. The interfacial gas liquid equilibrium is considered at boundary r_2 which was defined by dimensionless Henry's law constant H_d.

Table 3 Boundary conditions

Boundary	Condition	Boundary condition
Tube (gas)		
$\boldsymbol{z=0}$	Inlet gas conditions	$C_g = C_0$
$\boldsymbol{z=L}$	Convective flux at gas outlet	$-D_g\frac{\partial C_g}{\partial z}=0$
$\boldsymbol{r=0}$	Axial symmetry	$\frac{\partial C_g}{\partial r}=0$
$\boldsymbol{r=r_1}$	Interfacial continuity	$C_g = C_m$
Membrane (gas)		

$\boldsymbol{z = 0}$	No Flux	$-D_m \frac{\partial C_m}{\partial z} = 0$
$\boldsymbol{z = L}$	No Flux	$-D_m \frac{\partial C_m}{\partial z} = 0$
$\boldsymbol{r = r_1}$	Interfacial continuity	$C_m = C_g$
$\boldsymbol{r = r_2}$	Interfacial gas liquid equilibrium	$C_m = \frac{C_l}{H_d}$
Shell (liquid)		
$\boldsymbol{z = 0}$	Convective flux at liquid outlet	$-D_l \frac{\partial C_l}{\partial z} = 0$
$\boldsymbol{z = L}$	Inlet liquid conditions	$C_l = C_{r,out}$
$\boldsymbol{r = r_2}$	Interfacial gas liquid equilibrium	$C_{l=} H_d\ C_m$
$\boldsymbol{r = r_3}$	Axial symmetry	$\frac{\partial C_l}{\partial r} = 0$

3.2.3 Meshing and numerical resolution

An appropriate mesh is necessary for finite element analysis. For the current symmetrical geometry a refined mapped meshing was selected across the three domains. More refined mesh was applied inside the mesoporous membrane using for both rectangular shaped elements in accordance with the two directions (r, z) of the mass transport as presented in Figure S 1 of the supplementary data.

The set of equations presented in the preceding sections were coupled and solved using COMSOL Multiphysics® (version 5.3a, 2018) and MATLAB R2017a using LiveLink™ for MATLAB®. The finite element method was used which considers the piecewise polynomial interpolation over the domains and numerically resolves these equations at each of the nodes. A fully coupled process was applied with BDF time stepping and strict steps for the solver. The 2D equation system was scaled down axially due to a large difference between r and z directions and to prevent a high number of elements in the axial direction. Axial coordinate, length of the fiber, interstitial velocities and diffusion coefficients in axial direction were divided by the corresponding scale factor.

4 Results and discussion

4.1 ILs and membrane properties and characterization

4.1.1 IL properties and characterization

Various properties need to be considered for an absorbent to be used in membrane contactors, including viscosity, surface tension, CO_2 diffusivity, CO_2 solubility and thermal stability of the absorbent.

CO_2 solubility and inverse Henry's law constant (H_{px} (MPa), details in supplementary data), are important parameters to characterize the capacity of ILs for CO_2 absorption. A low value of the inverse Henry's law constant indicates very high gas solubility (Anthony et al., 2002; Lei et al., 2014). The magnitude of this constant also indicates the physical and chemical nature of the absorption. Smaller values of inverse Henry's law constant (H_{px} <3MPa) denote the chemical absorption nature of the absorbent for CO_2 (Wang et al., 2011; Yokozeki et al., 2008). Table 4 shows equilibrium concentration of CO_2 in IL at specified pressure and temperature and inverse Henry's law constants. According to the values reported in the

table (from literature), in terms of CO_2 solubility the four ILs are ranked as: [emim] [AC] > [emim] [$MeSO_4$] > [emim] [$EtSO_4$] > [emim] [DCA].

Viscosity is another important parameter, which affects the flow of absorbent in membrane contactors and also affects the diffusivity of CO_2 in the absorbent. A higher viscosity not only reduces the overall mass transfer coefficient but also increases the liquid side pressure drop in membrane contactors, especially when operating at low temperatures (Zhao et al., 2016). Among the ILs considered for this study, [emim] [DCA] has the lowest values of viscosity (4-6 times lower than other three ILs). Viscosities of ILs [emim] [DCA], [emim] [$MeSO_4$], [emim] [$EtSO_4$] and [emim] [AC] at 298 K are reported to be 15.1 mPa s, 78.1 mPa s, 97 mPa s and 141.1 mPa s, respectively. CO_2 diffusivities in ILs were calculated using the correlation (equation 7) developed by Morgan et al. (2005). This correlation confirms the inverse effect of the viscosity on CO_2 diffusivity. Other correlations developed for CO_2 diffusivity in ILs also confirm the strong dependency of CO_2 diffusivity on viscosity and their inverse relation (Moganty and Baltus, 2010; Moya et al., 2014; Ying and Baltus, 2007; Zubeir et al., 2015). Diffusivities of the ILs [emim] [DCA], [emim] [$MeSO_4$], [emim] [$EtSO_4$] and [emim] [AC] at 298 K are reported to be 1.15 10^{-5} cm^2 s^{-1}, 3.9 10^{-6} cm^2 s^{-1}, 3.38 10^{-6} cm^2 s^{-1} and 2.64 10^{-6} cm^2 s^{-1}, respectively. Diffusivity of [emim] [DCA] is one magnitude higher than diffusivities of other three ILs due to far lower viscosity compared to other ILs. In terms of viscosity and diffusivity these ILs can be ranked as [emim] [DCA] > [emim] [$MeSO_4$] > [emim] [$EtSO_4$] > [emim] [AC].

Surface tension is an important parameter for absorbents to be used with porous membrane contactors as it can describe the pore wetting resistance of membrane for absorbents and affects the LEP which is a critical parameter to prevent pore wetting of membrane (Zhao et al., 2016). Values of surface tension for all four ILs were measured by the method described in section 2.2 and reported in Table 4, the contact angle for water was also measured and reported as reference. Values of surface tension show a gradual decrease with increase in temperature. IL [emim] [$MeSO_4$] shows the highest surface tension of 52.6 mN m^{-1}at 288 K, among all ILs.

Table 4 Properties of ILs and parameters for CO_2 absorption

IL	T(K)	x*/P(MPa)	Ref.	H_{px} (MPa)	Ref.	ρ (g cm^{-3})	Ref.	μ (mPa s)	Ref.	D_{CO_2} (cm^2 s^{-1}) 10^6	Ref.	ϒ (mN m^{-1})	Ref.
[emim] [$MeSO_4$]	288	-	-	-	-	1.289	(Costa et al., 2011)	128.6	(Costa et al., 2011)	2.81	This Work	52.6	This Work
	298	0.089/0.63	(Yim et al., 2018)	7.1	(Sumon and Henni, 2011)	1.286	(Costa et al., 2011)	78.1	(Costa et al., 2011)	3.90	This Work	51.2	This Work
	313	0.089/0.75	(Yim et al., 2018)	-	-	1.275	(Costa et al., 2011)	42.9	(Costa et al., 2011)	5.80	This Work	50.5	This Work
[emim] [DCA]	288	-	-	-	-	1.114	(Klomfar et al., 2011)	19.5	(Larriba et al., 2013)	9.76	This Work	46.4	This Work
	298	0.015/0.15	(Huang and Peng, 2017)	10.1	(Huang and Peng, 2017)	1.108	(Klomfar et al., 2011)	15.1	(Larriba et al., 2013)	11.56	This Work	45.4	This Work
	313	0.011/0.15	(Huang and Peng, 2017)	14.6	(Huang and Peng, 2017)	1.098	(Klomfar et al., 2011)	10.2	(Larriba et al., 2013)	14.97	This Work	45.0	This Work
[emim] [$EtSO_4$]	288	-	-	-	-	1.241	(Gómez et al., 2006)	152.0	(Gómez et al., 2006)	2.51	This Work	46.8	This Work
	298	0.027/0.26	(Jalili et al., 2010)	9.7	(Jalili et al., 2010)	1.237	(Gómez et al., 2006)	97.0	(Gómez et al., 2006)	3.38	This Work	46.3	This Work

	313	0.024/0.27	(Jalili et al., 2010)	11.1	(Jalili et al., 2010)	1.227	(Gómez et al., 2006)	50.9	(Gómez et al., 2006)	5.18	This Work	45.2	This Work
[emim] [Ac]	288	-	-	-	-	1.105	(Nazet et al., 2015)	288.0	(Nazet et al., 2015)	1.65	This Work	47.3	This Work
	298	0.270/0.1	(Yokozeki et al., 2008)	$5\ 10^{-3}$	(Yokozeki et al., 2008)	1.099	(Nazet et al., 2015)	141.1	(Nazet et al., 2015)	2.64	This Work	46.8	This Work
	313	-	-	-	-	1.087	(Nazet et al., 2015)	78.2	(Nazet et al., 2015)	3.90	This Work	45.9	This Work

4.1.2 Membrane properties and characterization

Selection of membrane is also very important for membrane contactor gas liquid absorption process. In this study, a mesoporous hydrophobic polypropylene membrane is used. PP material is resistant to dissolution in solvents and is suitable for low temperature applications (Mansourizadeh and Ismail, 2009).

Surface morphology of membrane was characterized by SEM analysis to investigate effect of long-term contact between ILs and the membrane. The surface of the porous membrane was analyzed before and after immersion for 20 days in ILs. Wang et al. (2005) has reported significant changes in surface morphologies and degradation due to various solvents. In present work, however no evident changes can be observed for all ILs. Figure 2 shows SEM of the surface and porous structure of membrane before and after immersion in IL [emim][$MeSO_4$]. Similar effects were confirmed for other three ILs. These SEM confirm that there are no noticeable effects of ILs on surface and porous structure of PP membrane.

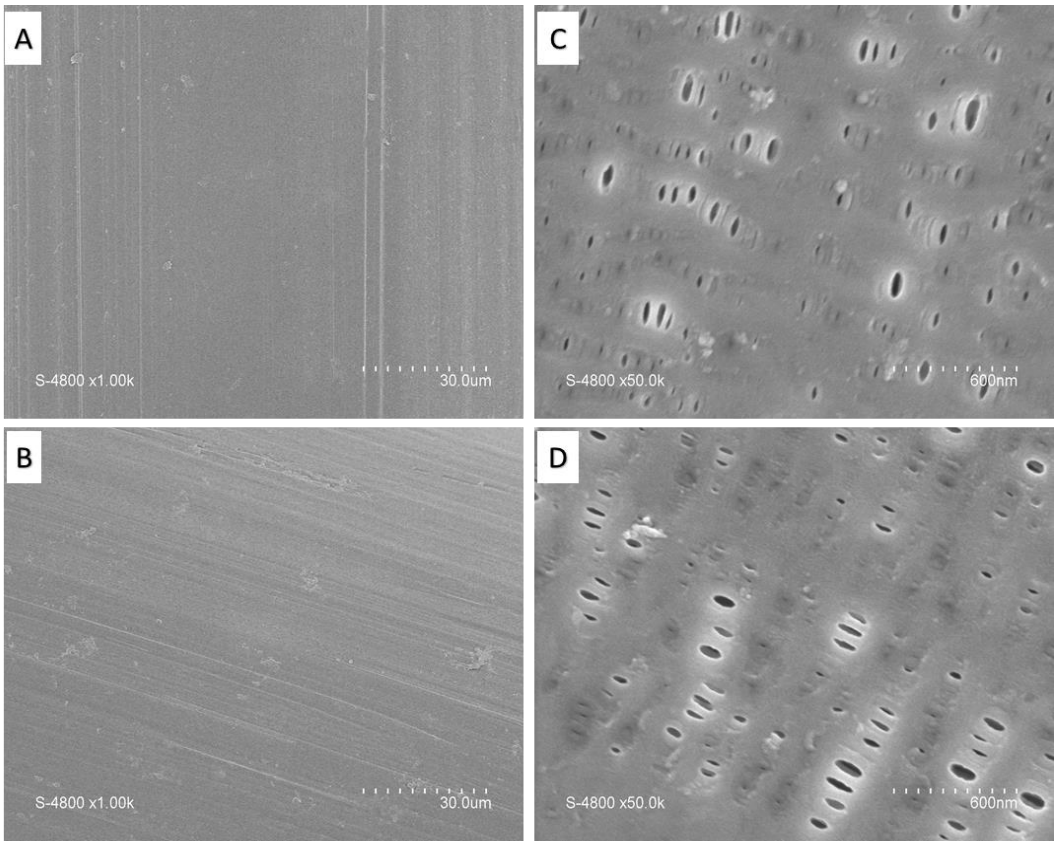

Figure 2. Scanning electron micrographs for (A) non-immersed PP fibers surface; (B) surface of PP fibers immersed for 20 days in [emim] [$MeSO_4$], (C) non-immersed PP fiber pores (D) pores of PP fibers immersed for 20 days in [emim] [$MeSO_4$]

Contact angle measurements were carried out to confirm the absence of pore wetting and of degradation due to solvent as suggested by SEM observations above. The contact angle represents the polarity difference between the membrane surface and the fluid (Gabelman and Hwang, 1999). Table 5 shows contact angles of four ILs and water before and after 40 days of immersion of fiber in ILs and water. Visuals of the measurements are presented in supplementary data Figure S 3. PP fibers were cleaned properly before measurements, and each angle was measured 15 times. PP fiber showed higher contact angle of 101.9^O with water. Contact angles measured for IL [emim] [$MeSO_4$] and [emim] [DCA] were higher than that of [emim] [$EtSO_4$] and [emim] [AC]. Before immersion the angles measure for [emim] [$MeSO_4$], [emim], [emim] [$EtSO_4$] and [emim] [AC] were 84.2^O, 82.9^O, 71.1^O and 72.9^O, respectively. There is only 1 ^{O} -2 ^{O} drop in contact angles measured after 40 days of immersion of fiber in ILs. LEP is another important parameter which is used to evaluate the wettability of porous membrane for liquid absorbents (Zhao et al., 2015a, 2015b). LEP defines the minimum pressure applied on the liquid to enter the membrane pores, which is estimated by Laplace-Young equation (Gabelman and Hwang, 1999; Kumar et al., 2002) given below.

$$LEP = \Delta P = -\frac{4B\Upsilon \cos\theta}{d_{max}} \quad (16)$$

Where B represents pore geometry coefficient (B=1 for cylindrical pores; 0 < B < 1 for non-cylindrical pores), θ is the contact angle between liquid absorbent and membrane and d_{max} is the maximum pore diameter of the membrane. According to Laplace-Young equation LEP is favored by smaller pore size and higher surface tensions. LEP of all ILs and water for membrane contactor (characteristics in Table 1) used in current study are presented in Table 5. Transmembrane pressure for the current absorption process in membrane contactor was kept lower than the measured LEP, to avoid wetting of the pores.

Table 5 Contact angle and LEP of ILs and PP membrane contactor

Absorbent	**Contact Angle (deg)**		**LEP(Bar)**
	Before immersion	**After immersion**	
[emim][$MeSO_4$]	84.2	82.2	1.95
[emim] [DCA]	82.9	81.0	2.19
[emim][$EtSO_4$]	71.1	71.0	5.70
[emim][Ac]	72.9	69.6	5.21
Water	101.9	-	5.65

4.2 CO_2 absorption in membrane contactor

CO_2 absorption experiments were carried out with four ILs coupled with PP membrane contactor and according to the method explained in section 3.3. Evolution of gas phase output concentration against operation time is presented in Figure S 4 and S 5 of the supplementary data. Efficiency of the absorption process was evaluated at different gas flow rates and process temperatures. CO_2 removal efficiency is

generally favored by lower gas flowrates. An increase in gas flowrate reduces the CO_2 removal efficiency due to minimal residence time of gas inside the contactor (Yan et al., 2007; Yeon et al., 2005). Despite the fact of reduction in efficiency with increase in gas flowrate, there is enhancement in the mass transfer due to greater average concentration of CO_2 on the gas side due to which the amount of CO_2 on the liquid side increases (Li and Chen, 2005; Zhang et al., 2006). The CO_2 removal efficiency was found from equation below.

$$Efficiency\ (\%) = \left(1 - \frac{C_{g-out}}{C_{g-in}}\right) 100 \tag{17}$$

Figure 3 shows CO_2 removal efficiency based on the output gas phase, at different gas flowrates.

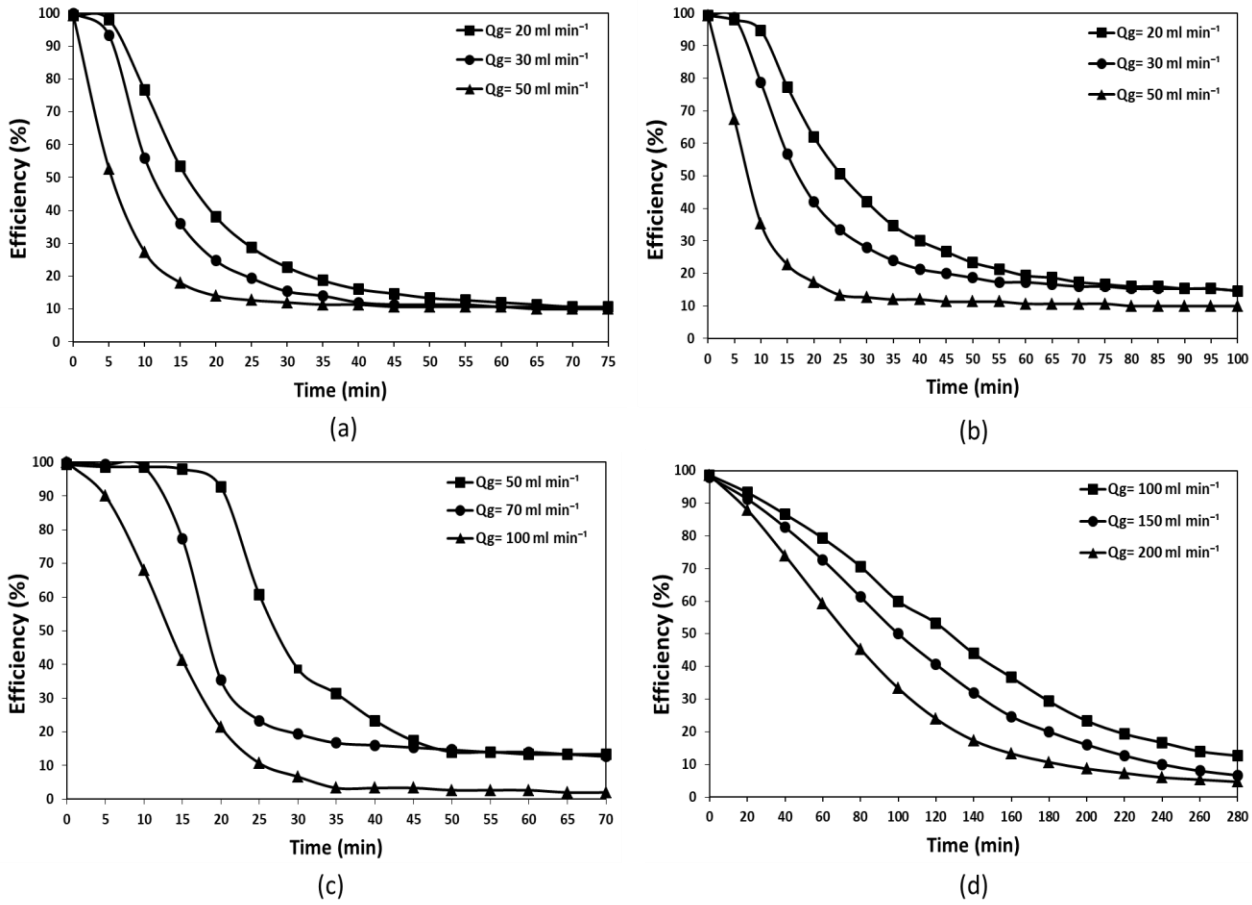

Figure 3. CO_2 removal efficiency against operation time for IL (a) [emim] [$MeSO_4$], (b), [emim] [DCA] (c) [emim] [$EtSO_4$] and (d) [emim] [Ac] at $T = 288\ K$ and $Q_{IL} = 60\ ml\ min^{-1}$.

Initially the CO_2 concentration at the output gas phase increases very fast and slows down with time until reaching pseudo-steady-state. At this stage, the increase in CO_2 concentration becomes very slow and concentration can be considered constant with time. At lower gas flowrates the efficiency remains almost 100%, initially, as the IL is able to absorb more CO_2. Absorption with IL [emim] [$EtSO_4$] shows 98% efficiency even after 20 minutes and 15 minutes of recirculation at gas flowrate of 50 ml.min^{-1} and 70 ml.min^{-1}, respectively. Generally, ILs dissolve a certain amount of CO_2, which is mostly considered to be physisorption for RTILs (Gurau et al., 2011; Maginn, 2005). However, the initial faster absorption can be

explained as of the complex formation at gas liquid interface, which is more chemical in nature, as the IL has very lower CO_2 concentration during initial recirculation. The absorption becomes slower with time due to physical absorption in the bulk of the liquid and due to lower diffusivities of the ILs, until it reaches pseudo-steady-state. Gas flowrate has evident effect on the outlet concentration and removal efficiency of CO_2. For ILs [emim] [$MeSO_4$] and [emim] [DCA] after 10 minutes, a decrease in removal efficiency of 43 % and 58 %, respectively, was observed by using 50 $ml.min^{-1}$ gas flowrate instead of 20 $ml.min^{-1}$. For [emim] [$EtSO_4$] after 10 minutes an efficiency drop of 28 % was recorded by increasing the gas flowrate from 50 $ml.min^{-1}$ to 100 $ml.min^{-1}$. After 60 minutes of recirculation, the efficiency drop for [emim] [AC] was 20 % by applying 200 $ml.min^{-1}$ gas flowrate instead of 100 $ml.min^{-1}$. Apart from few exceptions, the pseudo-steady-state efficiency was not much affected by the gas flowrate. IL [emim][AC] was observed to be far more efficient than other ILs, as even at the highest gas flowrate (200 $ml.min^{-1}$) it took 280 minutes to reach pseudo-steady-state. This phenomenon can also be confirmed from its very lower value of Henry constant (Table 4). Despite being a RTIL, CO_2 absorption in IL [emim] [AC] is considered to be chemisorption (Gurau et al., 2011; Yokozeki et al., 2008). Gas flowrates were selected for ILs according to their performance. ILs operated at low gas flow rates were not able to withstand absorption for enough time at high flowrates, while those operated at high gas flowrates were too slow to reach pseudo-steady-state at low gas flowrates.

ILs used are thermally stable and there is no effect on the vapor pressure in the investigated range of current study (results not presented here). Temperature has two opposite effects on the absorption of CO_2 in ILs. It decreases viscosity of the IL thus enhances CO_2 diffusivity in ILs (Table 4). But CO_2 solubility in RTILs is negatively affected by temperature. An increase in temperature reduces the CO_2 solubility and increases the inverse Henry's law constant (Lei et al., 2014; Okoturo and VanderNoot, 2004). Henry's law constant (Table 4) for IL [emim] [DCA] and [emim] [$EtSO_4$] increases from 10.1 MPa to 14.6 MPa and 9.7 MPa to 11.1 MPa, respectively, when temperature rises from 298 K to 313 K. Figure 4 shows the evolution of gas side outlet concentration of CO_2 at different temperatures. It is clear from the figure that increase in temperature has reduced the removal efficiency. However, the efficiency at pseudo-steady-state remains nearly unaffected. At 20 minutes of recirculation time, an efficiency drop of 12 %, 8 % and 31 % was observed for ILs [emim] [$MeSO_4$], [emim] [DCA] and [emim] [$EtSO_4$], respectively, for increasing temperature from 288 K to 313 K. For [emim] [AC] a drop of 17 % in removal efficiency can be observed, when temperature was changed from 288 K to 323 K, after 80 minutes.

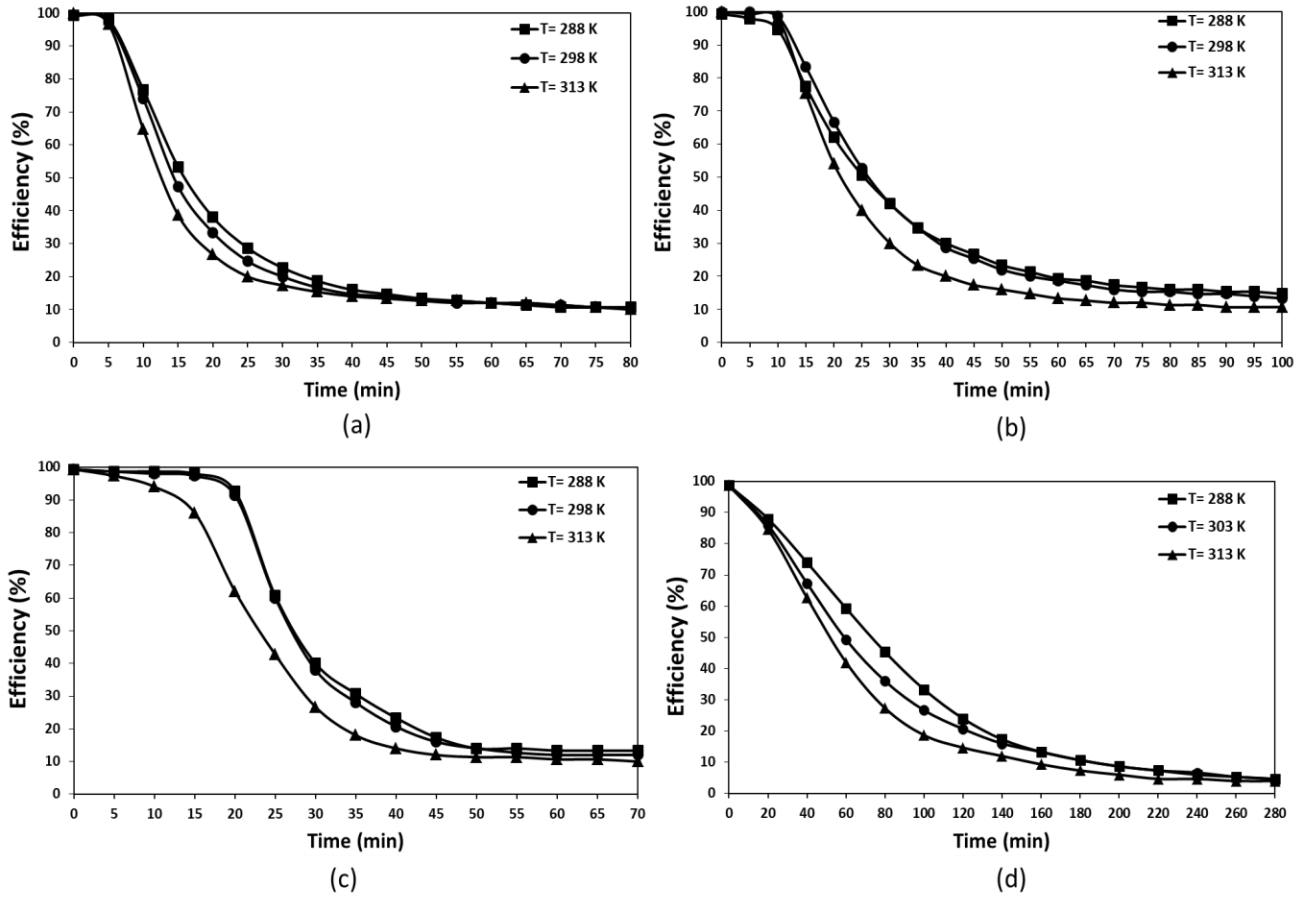

Figure 4. CO_2 removal efficiency against operation time for IL (a) [emim] [$MeSO_4$] ($Q_g = 20\ ml\ min^{-1}$), (b) [emim] [DCA] ($Q_g = 20\ ml\ min^{-1}$), (c) [emim] [$EtSO_4$] ($Q_g = 50\ ml\ min^{-1}$) and (d) [emim] [Ac] ($Q_g = 100\ ml\ min^{-1}$) at $Q_{IL} = 60\ ml\ min^{-1}$.

4.3 Mass transfer kinetics

4.3.1 Mass transfer coefficient and CO_2 flux: Effect of gas flowrate, temperature and CO_2 loading

As discussed in previous section, increase in gas flowrate enhances mass transfer of CO_2 and its concentration on the liquid side. This can be confirmed from Figure 5. Both mass transfer flux and experimental overall mass transfer coefficient increase with increase in gas flowrate. For both ILs [emim] [$MeSO_4$] and [emim] [DCA], initially, increasing gas flow rate from 20 ml min^{-1} to 50 ml min^{-1} increased CO_2 flux and experimental mass transfer coefficient from 1.2 10^{-5} mol m^{-2} s^{-1} to 3.1 10^{-5} mol m^{-2} s^{-1} and 9.3 10^{-6} m s^{-1} to 2.3 10^{-5} m s^{-1}, respectively. IL [emim] [$EtSO_4$] showed an increase from 3.1 10^{-5} mol m^{-2} s^{-1} to 6.2 10^{-5} mol m^{-2} s^{-1} and 2.3 10^{-5} m s^{-1} to 4.6 10^{-5} m s^{-1}, respectively, when gas flowrate was increased from 50 ml min^{-1} to 100 ml min^{-1}. For IL [emim] [AC] increasing gas flow rate from 100 ml min^{-1} to 200 ml min^{-1} increased CO_2 flux and experimental mass transfer coefficient from 6.2 10^{-5} mol m^{-2} s^{-1} to 1.2 10^{-4} mol m^{-2} s^{-1} and 4.6 10^{-5} m s^{-1} to 9.3 10^{-5} m s^{-1}, respectively. Liquid phase mass transfer coefficient remained unaffected by variations in gas flowrate.

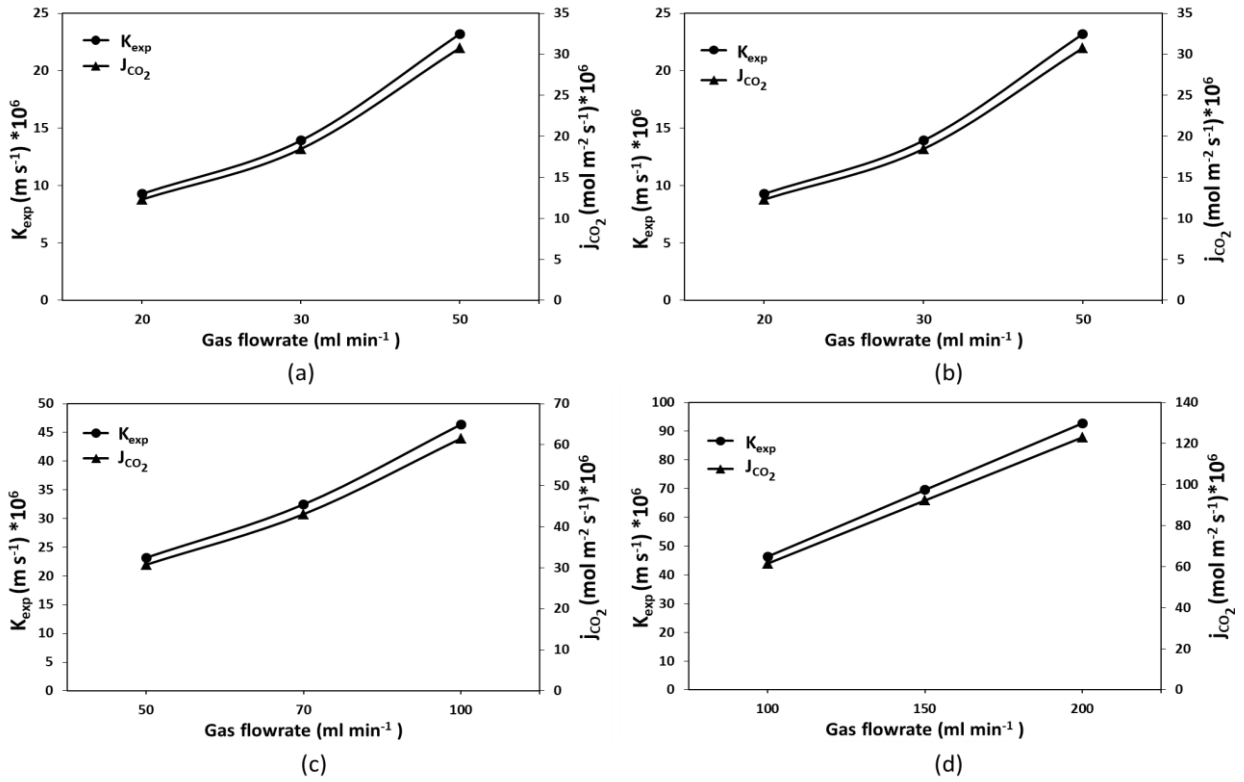

Figure 5. Effect of gas flowrate on CO_2 flux (j_{CO_2}) and experimental mass transfer coefficient (K_{exp}) for IL (a) [emim] [$MeSO_4$], (b), [emim] [DCA] (c) [emim] [$EtSO_4$] and (d) [emim] [Ac] at $T = 288\ K$ and $Q_{IL} = 60\ ml\ min^{-1}$.

As discussed previously, temperature affects both diffusion coefficient and Henry's law constant, which has opposite effects on mass transfer performance. To see the effect of temperature on mass transfer flux and experimental mass transfer coefficient values were taken after few minutes of recirculation. The effects can be observed in Figure 6. Both mass transfer flux and experimental mass transfer coefficient decrease with temperature ehancement. However, the effect is much smaller compared to gas flowrate. Liquid side mass transfer coefficient is a function of diffusivity, Reynolds number and Schmidt number (equation 5). Liquid side mass transfer coefficients show considerable amount of increase with increase in temperature as all the above-mentioned parameters are temperature dependent. For ILs [emim] [$MeSO_4$], [emim] [DCA], [emim] [$EtSO_4$] and [emim] [AC] liquid mass transfer coefficient increases from 2.3 10^{-6} m s^{-1} to 4.5 10^{-6} m s^{-1}, 1.7 10^{-6} m s^{-1} to 10.3 10^{-6} m s^{-1}, 2.1 10^{-6} m s^{-1} to 4.0 10^{-6} m s^{-1} and 1.4 10^{-6} m s^{-1} to 3.1 10^{-6} m s^{-1}, respectively by increasing temperature from 288 K to 313 K.

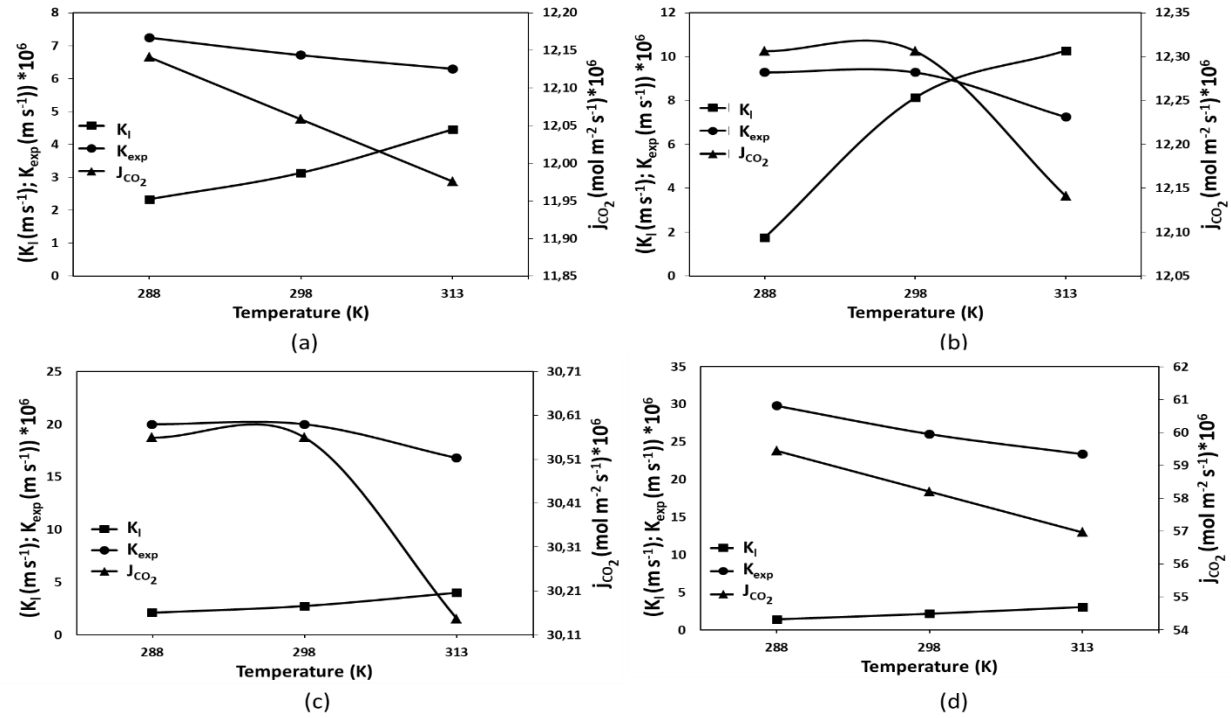

Figure 6. Effect of operation temperature on CO_2 flux (j_{CO_2}), experimental mass transfer coefficient (K_{exp}) and liquid mass transfer coefficient (K_l) for ILs (a) [emim] [$MeSO_4$] ($Q_g = 20\ ml\ min^{-1}$), (b) [emim] [DCA] ($Q_g = 20\ ml\ min^{-1}$), (c) [emim] [$EtSO_4$] ($Q_g = 50\ ml\ min^{-1}$) and (d) [emim] [Ac] ($Q_g = 100\ ml\ min^{-1}$) at $Q_{IL} = 60\ ml\ min^{-1}$.

CO_2 mass transfer flux and experimental mass transfer coefficients are continuously evolving with operation time as shown in Figure 7. These values decrease until it reaches a lower value at pseudo-steady-state where it becomes almost constant. It nearly takes 50-70 minutes for these values to be stable in case of [emim] [$MeSO_4$], [emim] [DCA] and [emim] [$EtSO_4$] while for [emim] [AC] the time to reach pseudo-steady-state is nearly 280 minutes. The driving force for the mass transfer here is concentration gradient which continuously evolves with operation time due to accumulation of CO_2 on the liquid side. Both mass transfer flux and experimental mass transfer coefficient depend upon the logarithmic mean of the driving force according to equation 9. Logarithmic mean of the driving force continuously evolves due to the evolution of CO_2 concentration in the gas phase (C_g^*) in equilibrium with the corresponding CO_2 concentration in the liquid phase (C_l^*). The equilibrium at gas liquid interface was defined by Henry's law constant.

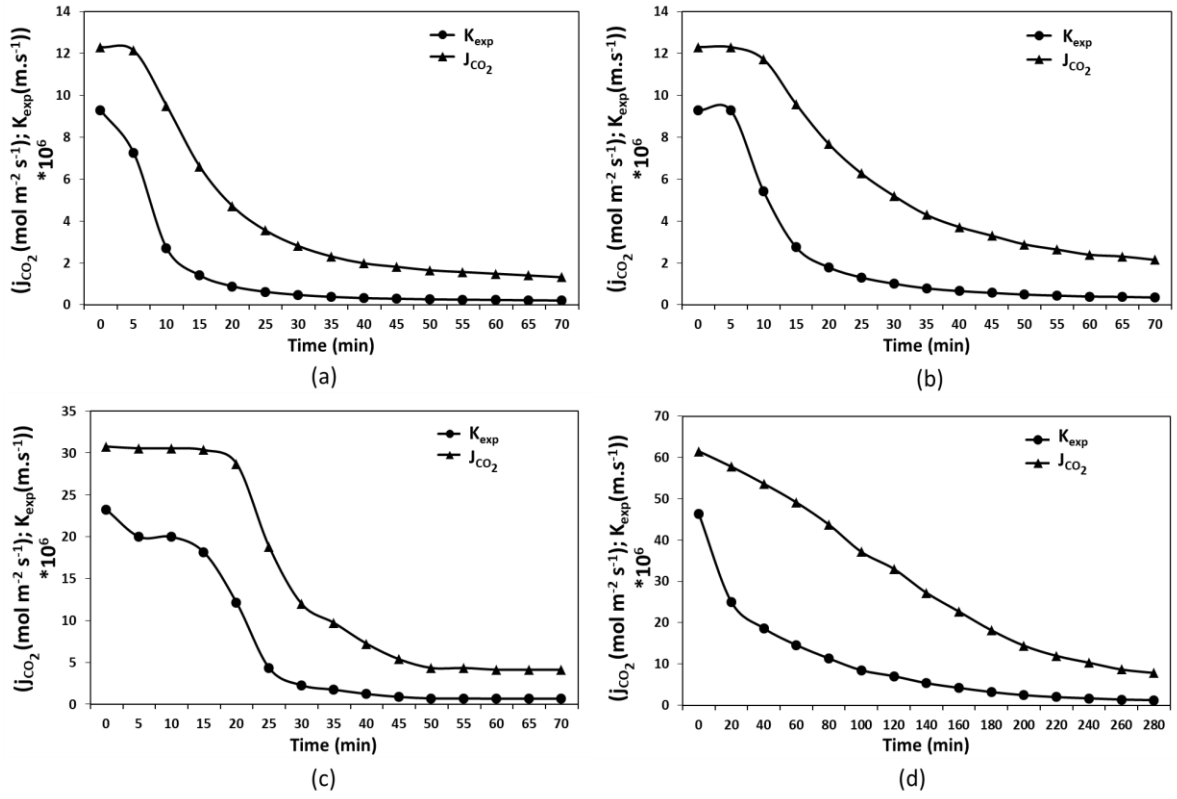

Figure 7. Variation of CO_2 flux (j_{CO_2}) and experimental mass transfer coefficient (K_{exp}) with operation time for four ILs (a) [emim] [$MeSO_4$] ($Q_g = 20\ ml\ min^{-1}$), (b) [emim] [DCA] ($Q_g = 20\ ml\ min^{-1}$), (c) [emim] [$EtSO_4$] ($Q_g = 50\ ml\ min^{-1}$) and (d) [emim] [Ac] ($Q_g = 100\ ml\ min^{-1}$) at $T = 288\ K$ and $Q_{IL} = 60\ ml\ min^{-1}$.

4.3.2 Enhancement factor and first order rate constant: Effect of CO_2 loading

During recirculation, ILs continuously absorbs CO_2, which accumulates on the shell side of the contactor. This accumulation slows down the gradient and then the mass transfer process and absorption kinetics as it has been explained in section 4.2. This phenomenon is explained here in terms of enhancement factor and first order rate constant. In Figure 8 we can notice that absorption rate changes with time. Initially CO_2 loading increases very rapidly but slows down with time as far as the number of recirculation loops increases. During the first ten minutes, [emim][$MeSO_4$], [emim][DCA] and [emim] [$EtSO_4$] absorbs respectively 56 %, 48 % and 48 % of the total CO_2 absorbed, the rest of the CO_2 is absorbed during the last 70 minutes of the process. In case of [emim][Ac], the total absorption time was 280 minutes out of which 34 % CO_2 was absorbed in first 10 minutes. The slow absorption rate of the ILs might be due to two reasons. Physical absorption in the bulk, which hinders the mass transfer due to high viscosity of ILs and low diffusivities and low driving force (concentration difference) due to high CO_2 loading in initial minutes. The enhancement factor is used to quantify the improvement of mass transfer due to the presence of chemical reaction. The results show strong dependency of the enhancement factor on CO_2 concentration in IL. It is evident from figure that the enhancement factor drops very rapidly in the first minutes of absorption and then slows down (almost reaches to a negligible value) as absorption reaches pseudo-steady-state. The decrease in enhancement factor shows that increase in CO_2 loading is reducing the mass transfer enhancement due to chemical reaction. The enhancement factor for IL [emim] [AC] is much

higher than other ILs. Based on the enhancement factor the mass transfer enhancement of CO_2 in these ILs can be ranked as [emim] [AC] >> [emim] [$EtSO_4$] > [emim] [$MeSO_4$] > [emim] [DCA]. First order rate constant is another parameter considered to predict the changes in the absorption behavior with increase in CO_2 concentration in ILs. The first order rate constant shows strong dependency on CO_2 concentration in ILs as it decreases very rapidly in the first minutes of absorption. Based on the first order rate constant the initial fast absorption can be considered as interfacial chemical absorption in which the mass transfer happens only at the interface. After enough recirculations of the IL, CO_2 absorption at the interface becomes negligibly small and CO_2 diffuses through the bulk of the ILs. Based on the first order rate constant, ILs can be ranked as [emim] [AC] > [emim] [$EtSO_4$] > [emim] [$MeSO_4$] > [emim] [DCA].

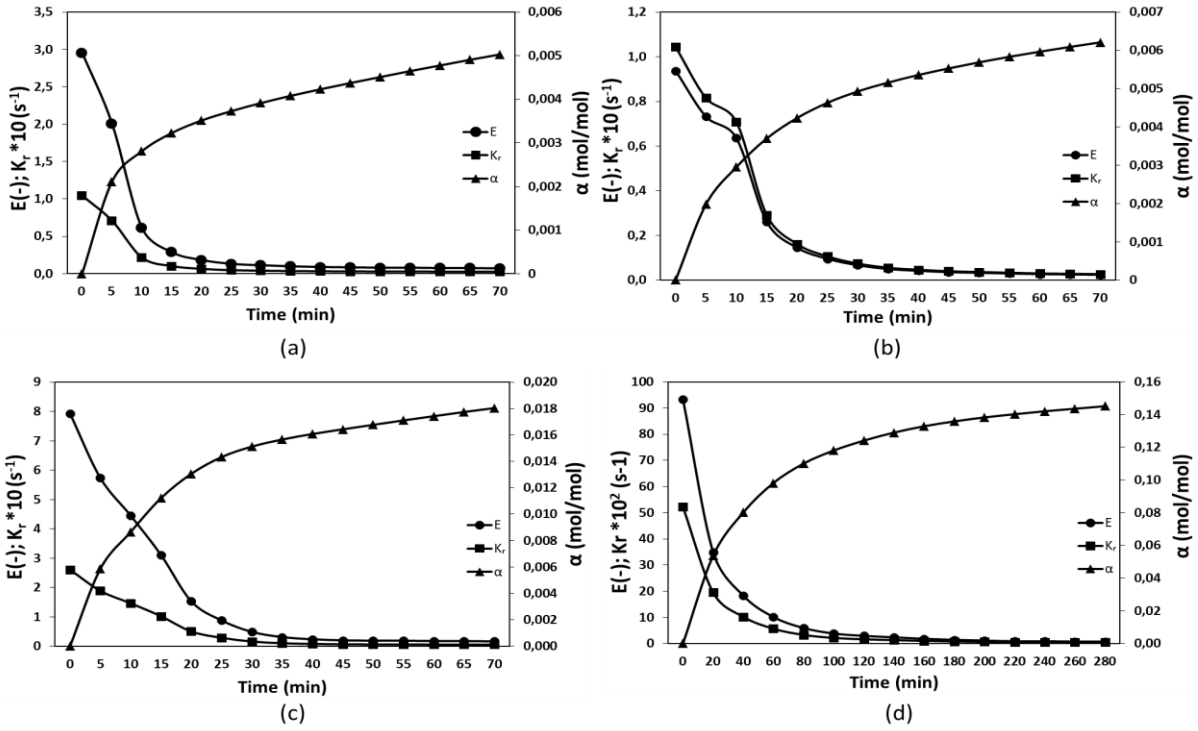

Figure 8. Evolution of enhancement factor (E), first order rate constant (K_r) and CO_2 loading (α) with operation time for IL (a) [emim] [$MeSO_4$], (b), [emim] [DCA] (c) [emim] [$EtSO_4$] and (d) [emim] [Ac] at $T = 313\ K$ and $Q_{IL} = 60\ ml\ min^{-1}$.

Table 6 shows values of experimental mass transfer coefficient, CO_2 loading of the ILs and enhancement factors at initial time (t_i) and when the absorption reaches steady state (t_s). A smaller increment in temperature has considerably affected the CO_2 loadings. The experimental mass transfer coefficient seems to be unaffected with increase in temperature, initially. After some recirculation this coefficient was reported to be lower at high temperatures. There was a significant decrease in enhancement factor with increase in temperature.

Table 6 CO_2 loading, experimental mass transfer coefficient and enhancement factor

IL	Q_g (ml min^{-1})	Time	100 α (mol mol^{-1})	K_{exp} (m s^{-1}) 10^6	E (-)
			T=298 K		
[$MeSO_4$]–	20	t_i	-	9.28	5.57

		t_s	0.55	0.22	0.13
[DCA]-	20	t_i	-	9.27	1.64
		t_s	0.72	0.32	0.057
[$EtSO_4$]-	50	t_i	-	23.31	18.71
		t_s	2.11	0.59	0.47
[Ac]-	100	t_i	-	46.40	122.50
		t_s	16.70	0.44	1.99
		T=313 K			
[$MeSO_4$]-	20	t_i	-	9.28	2.96
		t_s	0.51	0.22	0.07
[DCA]-	20	t_i	-	9.27	0.94
		t_s	0.62	0.24	0.02
[$EtSO_4$]-	50	t_i	-	23.20	7.93
		t_s	1.80	0.48	0.17
[Ac]-	100	t_i	-	46.37	93.32
		t_s	14.50	0.37	0.76

4.4 Modelling discussion

This section discusses the results obtained from the simulation of the 2D dynamic model developed for the experimental setup presented in the section 2.3. Fresh and unloaded ILs were considered for countercurrent recirculation through the shell side in a closed loop. Gas mixture (15 % CO_2 and N_2 rest to balance) was considered in open loop passing through the lumen side. Simulations of the variation in normalized gas side outlet concentration against time were plotted and compared with the experimental data, as presented in Figure 9. Operating conditions were adopted from Table 2 of the experimental section to compare the agreement between simulations and experimental data. The pseudo-steady-state 2D dynamic model was able to closely predict the experimental data within a range of 2-5 % standard deviation.

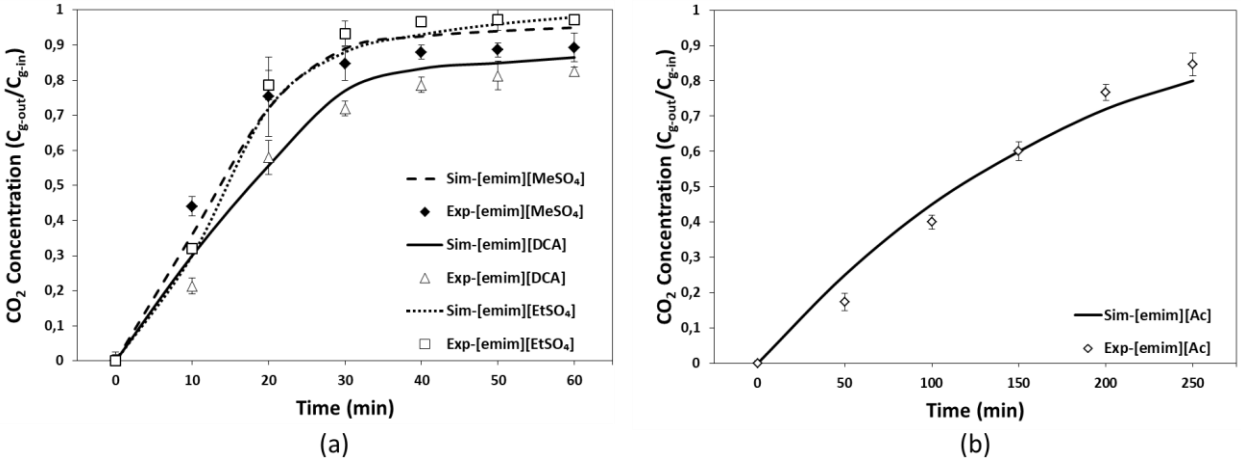

Figure 9 Comparison of simulation with experimental data under non-wetting assumption (a) [emim] [$MeSO_4$], [emim] [DCA] and [emim] [$EtSO_4$] at $Q_g = 50\ ml\ min^{-1}$ (b) [emim] [Ac] at $Q_g = 100\ ml\ min^{-1}; T = 288\ K, Q_{IL} = 60\ ml\ min^{-1}, CO_2\ concentartion = 15\ \%\ vol$

A sensitivity analysis was carried out for IL [emim] [$MeSO_4$]. As the IL was considered in a closed loop which leads the process to reach a pseudo-steady-state due to continuous loading of CO_2 to the IL. At pseudo-steady-state the CO_2 loading becomes very slow and constant. Operating time (IL recirculation time) to reach pseudo-steady-state is dependent upon the operating conditions which was analyzed in the current study against gas and liquid flowrates. Figure 10 presents dependency of the operation time to reach pseudo-steady-state upon gas and liquid flowrates. The results clearly demonstrated the dominancy of the gas flowrate over liquid flowrate. When the liquid flowrate was fixed at 40 ml min^{-1}, an increase in gas flowrate by 40 ml min^{-1} has decreased the operating time to reach pseudo-steady-state by 42 minutes. It clearly describes the increased mass transfer flux at higher gas flowrates which causes the IL to reach quickly to the target loading value. A decrease of only 4 minutes in operating time was observed by increasing liquid flowrate by 40 ml min^{-1}, at a fixed gas flowrate of 50 ml min^{-1}.

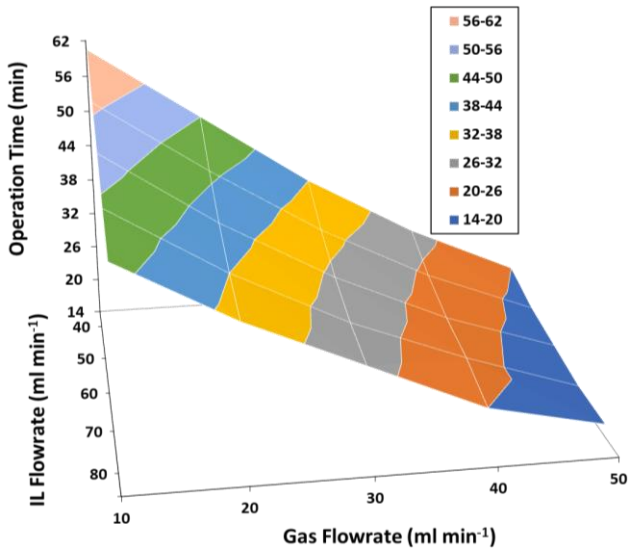

Figure 2 Dependency of the operating time over gas and liquid flowrates; $T = 288\ K$, $CO_2\ concentartion = 15\ \%\ vol.$

Although the assumptions of non-wetted membrane seem to be validated following the agreements of simulation and experimental results presented in Figure 9, a partial wetting analysis was carried out to observe its effect on the CO_2 flux and IL loading for long term operatibility. Long term operations and pressure variations can cause penetration of the liquid into the pores of porous membrane causing partial wetting of the membrane and leading to a huge drop in the CO_2 flux. Penetration of the viscous IL into the pores of the membrane can lead to a zero flux across the membrane if the wetting dominates the membrane. Figure 11 demonstrates the effect of partial wetting on the CO_2 flux and maximal IL loading after 60 minutes of operation. It's very clear that the effect is much stronger in the beginning as a drop of nearly one half of the flux was noted for 5 % wetting of the membrane. The drop in the mass transfer flux affects the accumulation of CO_2/CO_2 loading in the IL. The maximal CO_2 loading (60 minutes of operation time) decreases by 67 % when the membrane is 20 % wetted compared to non-wetted membrane.

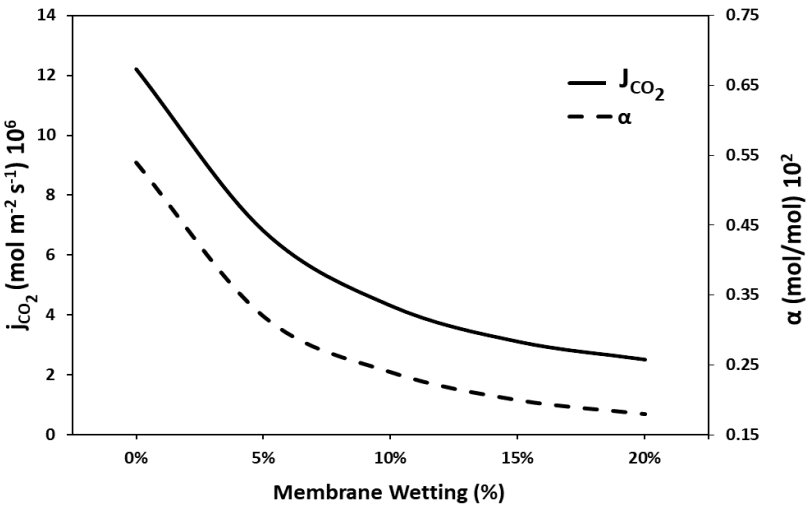

Figure 11 Effect of partial wetting of the membrane on CO_2 flux and IL loading; $Q_g = 20\ ml\ min^{-1}$; $Q_{IL} = 60\ ml\ min^{-1}, T = 288\ K, CO_2\ concentartion = \ 15\ \%\ vol$

5 Conclusion

This work investigates the separation performance of four [emim] cation based ILs coupled with PP membrane contactor in a closed loop for post-combustion CO_2 capture at moderate temperature and pressure. A detailed analysis of pseudo-steady-state absorption process and variations in absorption kinetics with increase in CO_2 concentration of the IL in membrane contactor was conducted. A dynamic modelling approach was also implemented to predict the pseudo-steady-state experimental behavior of the system. These ILs were screened and characterized based on thermogravimetric analysis, viscosity and surface tension measurements and CO_2 solubilities. SEM analysis of the fibers, contact angle of the ILs with the fiber and LEP were measured to ensure no wetting and degradability of the fibers and efficient coupling of the ILs with the membrane contactor. As the absorption experiments were performed at moderate pressure and transmembrane pressure was kept below LEP, no considerable wetting was witnessed, and the results were highly reproducible after long-term operations on a membrane contactor. Very high CO_2 mass transfer flux and experimental mass transfer coefficients were obtained during initial recirculation of the ILs. The absorption process was pseudo-steady-state in which the absorption rate was continuously evolving due to the accumulation of CO_2 on the liquid side leading to a decrease in driving force for mass transfer and other absorption kinetics of the ILs. The absorption process with the passage of operation time, lead to reach a steady state where the absorption rate became nearly constant. The absorption performance was more affected by gas flowrate and less affected by operation temperature. The absorption behavior was also investigated based on enhancement factor and first order rate constant. Based on the results, the initial faster absorption can be attributed as gas liquid interfacial chemisorption where the enhancement factor and first order rate constant were much higher compared to its values at higher operation times. The huge drop in these values confirmed the later absorption to be shifted to the bulk of the liquid which is mostly dependent on the diffusivity of the CO_2 in ILs. Although these ILs showed better absorption performance, another work on ILs and water mixtures and coupled absorption-desorption process is under study.

References

Albo, J., Luis, P., Irabien, A., 2010. Carbon Dioxide Capture from Flue Gases Using a Cross-Flow Membrane

Contactor and the Ionic Liquid 1-Ethyl-3-methylimidazolium Ethylsulfate. Ind. Eng. Chem. Res. 49, 11045–11051. https://doi.org/10.1021/ie1014266

Almeida, H.F.D., Teles, A.R.R., Lopes-Da-Silva, J.A., Freire, M.G., Coutinho, J.A.P., 2012. Influence of the anion on the surface tension of 1-ethyl-3- methylimidazolium-based ionic liquids. J. Chem. Thermodyn. 54, 49–54. https://doi.org/10.1016/j.jct.2012.03.008

Anthony, J.L., Maginn, E.J., Brennecke, J.F., 2002. Solubilities and thermodynamic properties of gases in the ionic liquid 1-n-butyl-3-methylimidazolium hexafluorophosphate. J. Phys. Chem. B. https://doi.org/10.1021/jp020631a

Barker, T., 2007. Climate Change 2007 : An Assessment of the Intergovernmental Panel on Climate Change, An Assessment of the Intergovernmental Panel on Climat Change. https://doi.org/10.1256/004316502320517344

Blath, J., Christ, M., Deubler, N., Hirth, T., Schiestel, T., 2011. Gas solubilities in room temperature ionic liquids - Correlation between RTiL-molar mass and Henry's law constant. Chem. Eng. J. https://doi.org/10.1016/j.cej.2011.05.084

Blath, J., Deubler, N., Hirth, T., Schiestel, T., 2012. Chemisorption of carbon dioxide in imidazolium based ionic liquids with carboxylic anions. Chem. Eng. J. 181–182, 152–158. https://doi.org/10.1016/j.cej.2011.11.042

Carvalho, P.J., Regueira, T., Fernández, J., Lugo, L., Safarov, J., Hassel, E., Coutinho, J.A.P., 2014. High pressure density and solubility for the CO2 + 1-ethyl-3-methylimidazolium ethylsulfate system. J. Supercrit. Fluids. https://doi.org/10.1016/j.supflu.2014.01.011

Chabanon, E., Bounaceur, R., Castel, C., Rode, S., Roizard, D., Favre, E., 2015. Pushing the limits of intensified CO2 post-combustion capture by gas-liquid absorption through a membrane contactor. Chem. Eng. Process. Process Intensif. https://doi.org/10.1016/j.cep.2015.03.002

Chau, J., Jie, X., Sirkar, K.K., 2016. Polyamidoamine-facilitated poly(ethylene glycol)/ionic liquid based pressure swing membrane absorption process for CO2 removal from shifted syngas. Chem. Eng. J. https://doi.org/10.1016/j.cej.2015.09.120

Chau, J., Obuskovic, G., Jie, X., Sirkar, K.K., 2014. Pressure swing membrane absorption process for shifted syngas separation: Modeling vs. experiments for pure ionic liquid. J. Memb. Sci. 453, 61–70. https://doi.org/10.1016/j.memsci.2013.10.038

Chen, Y., Zhang, S., Yuan, X., Zhang, Y., Zhang, X., Dai, W., Mori, R., 2006. Solubility of CO2 in imidazolium-based tetrafluoroborate ionic liquids. Thermochim. Acta. https://doi.org/10.1016/j.tca.2005.11.023

Constantinou, A., Barrass, S., Gavriilidis, A., 2014. CO2 absorption in polytetrafluoroethylene membrane microstructured contactor using aqueous solutions of amines. Ind. Eng. Chem. Res. https://doi.org/10.1021/ie403444t

Costa, A.J.L., Esperanca, M.S.S., Marrucho, I.M., Rebelo, L.P.N., 2011. Densities and Viscosities of 1-Ethyl-3-methylimidazolium n -Alkyl Sulfates. J. Chem. Eng. Data 56, 3433–3441.

Dai, Z., Ansaloni, L., Deng, L., 2016a. Precombustion CO_2 Capture in Polymeric Hollow Fiber Membrane Contactors Using Ionic Liquids: Porous Membrane versus Nonporous Composite Membrane. Ind. Eng. Chem. Res. 55, 5983–5992. https://doi.org/10.1021/acs.iecr.6b01247

Dai, Z., Deng, L., 2016. Membrane absorption using ionic liquid for pre-combustion CO2 capture at elevated pressure and temperature. Int. J. Greenh. Gas Control 54, 59–69. https://doi.org/10.1016/j.ijggc.2016.09.001

Dai, Z., Noble, R.D., Gin, D.L., Zhang, X., Deng, L., 2016b. Combination of ionic liquids with membrane technology: A new approach for CO2separation. J. Memb. Sci. 497, 1–20. https://doi.org/10.1016/j.memsci.2015.08.060

Dindore, V.Y., Brilman, D.W.F., Geuzebroek, R.H., Versteeg, G.F., 2004. Membrane-solvent selection for CO2 removal using membrane gas-liquid contactors. Sep. Purif. Technol. https://doi.org/10.1016/j.seppur.2004.01.014

Dindore, V.Y., Versteeg, G.F., 2005. Gas-liquid mass transfer in a cross-flow hollow fiber module: Analytical model and experimental validation. Int. J. Heat Mass Transf. https://doi.org/10.1016/j.ijheatmasstransfer.2005.03.002

Falk-Pedersen, O., Grønvold, M.S., Nøkleby, P., Bjerve, F., Svendsen, H.F., 2005. CO 2 Capture with Membrane Contactors . Int. J. Green Energy. https://doi.org/10.1081/ge-200058965

Figueroa, J.D., Fout, T., Plasynski, S., McIlvried, H., Srivastava, R.D., 2008. Advances in CO2 capture technology-The U.S. Department of Energy's Carbon Sequestration Program. Int. J. Greenh. Gas Control. https://doi.org/10.1016/S1750-5836(07)00094-1

Fröba, A.P., Kremer, H., Leipertz, A., 2008. Density, Refractive Index, Interfacial Tension, and Viscosity of Ionic Liquids [EMIM][EtSO 4], [EMIM][NTf 2], [EMIM][N(CN) 2], and [OMA][NTf 2] in Dependence on Temperature at Atmospheric Pressure. J. Phys. Chem. B 112, 12420–12430. https://doi.org/10.1021/jp804319a

Fuller, E.N., Schettler, P.D., Giddings, J.C., 1966. A new method for prediction of binary gas-phase diffusion coefficients. Ind. Eng. Chem. 58, 18–27. https://doi.org/10.1021/ie50677a007

Gabelman, A., Hwang, S.-T., 1999. Hollow fiber membrane contactors. J. Memb. Sci. 159, 61–106. https://doi.org/10.1016/S0376-7388(99)00040-X

Gómez-Coma, L., Garea, A., Irabien, A., 2014. Non-dispersive absorption of CO2in [emim][EtSO4] and [emim][Ac]: Temperature influence. Sep. Purif. Technol. 132, 120–125. https://doi.org/10.1016/j.seppur.2014.05.012

Gómez, E., González, B., Calvar, N., Tojo, E., Domínguez, Á., 2006. Physical Properties of Pure 1-Ethyl-3-methylimidazolium Ethylsulfate and Its Binary Mixtures with Ethanol and Water at Several Temperatures. J. Chem. Eng. Data 51, 2096–2102. https://doi.org/10.1021/je060228n

Gurau, G., Rodríguez, H., Kelley, S.P., Janiczek, P., Kalb, R.S., Rogers, R.D., 2011. Demonstration of chemisorption of carbon dioxide in 1,3-dialkylimidazolium acetate ionic liquids. Angew. Chemie - Int. Ed. 50, 12024–12026. https://doi.org/10.1002/anie.201105198

Hajilary, N., Rezakazemi, M., 2018. CFD modeling of CO2 capture by water-based nanofluids using hollow fiber membrane contactor. Int. J. Greenh. Gas Control. https://doi.org/10.1016/j.ijggc.2018.08.002

Happel, J., 1959. Viscous flow relative to arrays of cylinders. AIChE J. 5, 174–177. https://doi.org/10.1002/aic.690050211

Huang, K., Peng, H.L., 2017. Solubilities of Carbon Dioxide in 1-Ethyl-3-methylimidazolium Thiocyanate, 1-Ethyl-3-methylimidazolium Dicyanamide, and 1-Ethyl-3-methylimidazolium Tricyanomethanide at (298.2 to 373.2) K and (0 to 300.0) kPa. J. Chem. Eng. Data. https://doi.org/10.1021/acs.jced.7b00476

Iliuta, I., Bougie, F., Iliuta, M.C., 2015. CO2 removal by single and mixed amines in a hollow-fiber membrane module-investigation of contactor performance. AIChE J. https://doi.org/10.1002/aic.14678

Iversen, S.B., Bhatia, V.K., Dam-Johansen, K., Jonsson, G., 1997. Characterization of microporous membranes for use in membrane contactors. J. Memb. Sci. https://doi.org/10.1016/S0376-7388(97)00026-4

Jalili, A.H., Mehdizadeh, A., Shokouhi, M., Ahmadi, A.N., Hosseini-Jenab, M., Fateminassab, F., 2010. Solubility and diffusion of CO2and H2S in the ionic liquid 1-ethyl-3-methylimidazolium ethylsulfate. J. Chem. Thermodyn. 42, 1298–1303. https://doi.org/10.1016/j.jct.2010.05.008

Jie, X., Chau, J., Obuskovic, G., Sirkar, K.K., 2013. Preliminary studies of CO2 removal from precombustion syngas through pressure swing membrane absorption process with ionic liquid as absorbent. Ind. Eng. Chem. Res. 52, 8783–8799. https://doi.org/10.1021/ie302122s

Klomfar, J., Součková, M., Pátek, J., 2011. Temperature dependence of the surface tension and density at 0.1 MPa for 1-ethyl- and 1-butyl-3-methylimidazolium dicyanamide. J. Chem. Eng. Data. https://doi.org/10.1021/je200502j

Kumar, P.S., Hogendoorn, J.A., Feron, P.H.M., Versteeg, G.F., 2002. New absorption liquids for the removal of CO2 from dilute gas streams using membrane contactors. Chem. Eng. Sci. https://doi.org/10.1016/S0009-2509(02)00041-6

Larriba, M., Navarro, P., García, J., Rodríguez, F., 2013. Liquid-liquid extraction of toluene from heptane using [emim][DCA], [bmim][DCA], and [emim][TCM] ionic liquids. Ind. Eng. Chem. Res. 52, 2714–2720. https://doi.org/10.1021/ie303357s

Lei, Z., Dai, C., Chen, B., 2014. Gas solubility in ionic liquids. Chem. Rev. 114, 1289–1326. https://doi.org/10.1021/cr300497a

Li, J., Dai, Z., Usman, M., Qi, Z., Deng, L., 2016. CO2/H2 separation by amino-acid ionic liquids with polyethylene glycol as co-solvent. Int. J. Greenh. Gas Control. https://doi.org/10.1016/j.ijggc.2015.12.027

Li, J.L., Chen, B.H., 2005. Review of CO2absorption using chemical solvents in hollow fiber membrane contactors. Sep. Purif. Technol. 41, 109–122. https://doi.org/10.1016/j.seppur.2004.09.008

Lu, J., Wang, L., Sun, X., Li, J., Liu, X., 2005. Absorption of CO2 into aqueous solutions of methyldiethanolamine and activated methyldiethanolamine from a gas mixture in a hollow fiber contactor. Ind. Eng. Chem. Res. https://doi.org/10.1021/ie058023f

Lu, J.G., Ge, H., Chen, Y., Ren, R.T., Xu, Y., Zhao, Y.X., Zhao, X., Qian, H., 2017. CO2capture using a functional protic ionic liquid by membrane absorption. J. Energy Inst. 90, 933–940. https://doi.org/10.1016/j.joei.2016.08.001

Lu, J.G., Hua, A.C., Xu, Z.W., Li, J.T., Liu, S.Y., Wang, Z.L., Zhao, Y.L., Pan, C., 2013. CO2capture by membrane

absorption coupling process: Experiments and coupling process evaluation. J. Memb. Sci. 431, 9–18. https://doi.org/10.1016/j.memsci.2012.12.039
Lu, J.G., Lu, C.T., Chen, Y., Gao, L., Zhao, X., Zhang, H., Xu, Z.W., 2014. CO2capture by membrane absorption coupling process: Application of ionic liquids. Appl. Energy 115, 573–581. https://doi.org/10.1016/j.apenergy.2013.10.045
Lu, J.G., Lu, Z.Y., Chen, Y., Wang, J.T., Gao, L., Gao, X., Tang, Y.Q., Liu, D.G., 2015. CO<inf>2</inf> absorption into aqueous blends of ionic liquid and amine in a membrane contactor. Sep. Purif. Technol. 150, 278–285. https://doi.org/10.1016/j.seppur.2015.07.010
Luis, P., Garea, A., Irabien, A., 2009. Zero solvent emission process for sulfur dioxide recovery using a membrane contactor and ionic liquids. J. Memb. Sci. 330, 80–89. https://doi.org/10.1016/j.memsci.2008.12.046
Maginn, E.J., 2005. Design and evaluation of ionic liquids as novel CO2 absorbents, 2005. Univ. Norte Dame Notre Dame. https://doi.org/10.2172/859167
Mansourizadeh, A., Ismail, A.F., 2009. Hollow fiber gas-liquid membrane contactors for acid gas capture: A review. J. Hazard. Mater. https://doi.org/10.1016/j.jhazmat.2009.06.026
Mejía, I., Stanley, K., Canales, R., Brennecke, J.F., 2013. On the high-pressure solubilities of carbon dioxide in several ionic liquids. J. Chem. Eng. Data 58, 2642–2653. https://doi.org/10.1021/je400542b
Moganty, S.S., Baltus, R.E., 2010. Diffusivity of Carbon Dioxide in Room-Temperature Ionic Liquids. Ind. Eng. Chem. Res. 49, 9370–9376. https://doi.org/10.1021/ie101260j
Morgan, D., Ferguson, L., Scovazzo, P., 2005. Diffusivities of gases in room-temperature ionic Liquids: Data and correlations obtained using a lag-time technique. Ind. Eng. Chem. Res. 44, 4815–4823. https://doi.org/10.1021/ie048825v
Mosadegh-Sedghi, S., Rodrigue, D., Brisson, J., Iliuta, M.C., 2014. Wetting phenomenon in membrane contactors - Causes and prevention. J. Memb. Sci. https://doi.org/10.1016/j.memsci.2013.09.055
Moya, C., Palomar, J., Gonzalez-Miquel, M., Bedia, J., Rodriguez, F., 2014. Diffusion Coefficients of CO2 in Ionic Liquids Estimated by Gravimetry. Ind. Eng. Chem. Res. 53, 13782–13789. https://doi.org/10.1021/ie501925d
Nazet, A., Sokolov, S., Sonnleitner, T., Makino, T., Kanakubo, M., Buchner, R., 2015. Densities, Viscosities, and Conductivities of the Imidazolium Ionic Liquids [Emim][Ac], [Emim][FAP], [Bmim][BETI], [Bmim][FSI], [Hmim][TFSI], and [Omim][TFSI]. J. Chem. Eng. Data 60, 2400–2411. https://doi.org/10.1021/acs.jced.5b00285
Okoturo, O.O., VanderNoot, T.J., 2004. Temperature dependence of viscosity for room temperature ionic liquids. J. Electroanal. Chem. 568, 167–181. https://doi.org/10.1016/j.jelechem.2003.12.050
Ortiz, A., Gorri, D., Irabien, Á., Ortiz, I., 2010. Separation of propylene/propane mixtures using Ag+-RTIL solutions. Evaluation and comparison of the performance of gas-liquid contactors. J. Memb. Sci. 360, 130–141. https://doi.org/10.1016/j.memsci.2010.05.013
Papatryfon, X.L., Heliopoulos, N.S., Molchan, I.S., Zubeir, L.F., Bezemer, N.D., Arfanis, M.K., Kontos, A.G., Likodimos, V., Iliev, B., Romanos, G.E., Falaras, P., Stamatakis, K., Beltsios, K.G., Kroon, M.C., Thompson, G.E., Klöckner, J., Schubert, T.J.S., 2014. CO2 capture efficiency, corrosion properties, and ecotoxicity evaluation of amine solutions involving newly synthesized ionic liquids. Ind. Eng. Chem. Res. https://doi.org/10.1021/ie501897d
Qazi, S., Gómez-coma, L., Albo, J., Druon-bocquet, S., Irabien, A., 2020a. CO 2 capture in a hollow fiber membrane contactor coupled with ionic liquid : Influence of membrane wetting and process parameters. Sep. Purif. Technol. 233, 115986. https://doi.org/10.1016/j.seppur.2019.115986
Qazi, S., Manuel Vadillo, J., Gómez-Coma, L., Albo, J., Druon-Bocquet, S., Irabien, A., Sanchez-Marcano, J., 2020b. CO2 Capture with Room Temperature Ionic Liquids; Coupled Absorption/Desorption and Single Module Absorption in Membrane Contactor. Chem. Eng. Sci. https://doi.org/10.1016/j.ces.2020.115719
Quijada-Maldonado, E., Van Der Boogaart, S., Lijbers, J.H., Meindersma, G.W., De Haan, A.B., 2012. Experimental densities, dynamic viscosities and surface tensions of the ionic liquids series 1-ethyl-3-methylimidazolium acetate and dicyanamide and their binary and ternary mixtures with water and ethanol at T = (298.15 to 343.15 K). J. Chem. Thermodyn. 51, 51–58. https://doi.org/10.1016/j.jct.2012.02.027
Ramdin, M., De Loos, T.W., Vlugt, T.J.H., 2012. State-of-the-art of CO \n 2 capture with ionic liquids. Ind. Eng. Chem. Res. 51, 8149–8177. https://doi.org/10.1021/ie3003705
Rangwala, H.A., 1996. Absorption of carbon dioxide into aqueous solutions using hollow fiber membrane contactors. J. Memb. Sci. https://doi.org/10.1016/0376-7388(95)00293-6
Razavi, S.M.R., Rezakazemi, M., Albadarin, A.B., Shirazian, S., 2016. Simulation of CO2 absorption by solution of

ammonium ionic liquid in hollow-fiber contactors. Chem. Eng. Process. Process Intensif. https://doi.org/10.1016/j.cep.2016.07.001
Rezakazemi, M., Darabi, M., Soroush, E., Mesbah, M., 2019. CO2 absorption enhancement by water-based nanofluids of CNT and SiO2 using hollow-fiber membrane contactor. Sep. Purif. Technol. https://doi.org/10.1016/j.seppur.2018.09.005
Rezakazemi, M., Sadrzadeh, M., Matsuura, T., 2018. Thermally stable polymers for advanced high-performance gas separation membranes. Prog. Energy Combust. Sci. https://doi.org/10.1016/j.pecs.2017.11.002
Sander, R., 2015. Compilation of Henry's law constants (version 4.0) for water as solvent. Atmos. Chem. Phys. 15, 4399–4981. https://doi.org/10.5194/acp-15-4399-2015
Santos, C.S., Baldelli, S., 2009. Alkyl Chain Interaction at the Surface of Room Temperature Ionic Liquids: Systematic Variation of Alkyl Chain Length ($R = C_1 - C_4, C_8$) in both Cation and Anion of [RMIM][$R - OSO_3$] by Sum Frequency G. J. Phys. Chem. B 113, 923–933. https://doi.org/10.1021/jp807924g
Shen, S., Kentish, S.E., Stevens, G.W., 2010. Shell-side mass-transfer performance in hollow-fiber membrane contactors. Solvent Extr. Ion Exch. https://doi.org/10.1080/07366299.2010.515176
Sohaib, Q., Muhammad, A., Younas, M., Rezakazemi, M., 2020. Modelling Pre-Combustion CO2 Capture with Tubular Membrane Contactor Using Ionic Liquids at Elevated Temperatures. Sep. Purif. Technol. 116677. https://doi.org/10.1016/j.seppur.2020.116677
Soriano, A.N., Doma, B.T., Li, M.H., 2009. Carbon dioxide solubility in some ionic liquids at moderate pressures. J. Taiwan Inst. Chem. Eng. 40, 387–393. https://doi.org/10.1016/j.jtice.2008.12.002
Sumon, K.Z., Henni, A., 2011. Ionic liquids for CO2 capture using COSMO-RS: Effect of structure, properties and molecular interactions on solubility and selectivity. Fluid Phase Equilib. https://doi.org/10.1016/j.fluid.2011.06.038
Wang, G., Hou, W., Xiao, F., Geng, J., Wu, Y., Zhang, Z., 2011. Low viscosity triethylbutylammonium acetate as a task-specific ionic liquid for reversible CO2 absorption. J. Chem. Eng. Data 56, 1125–1133. https://doi.org/10.1021/je101014q
Wang, R., Zhang, H.Y., Feron, P.H.M., Liang, D.T., 2005. Influence of membrane wetting on CO2 capture in microporous hollow fiber membrane contactors. Sep. Purif. Technol. 46, 33–40. https://doi.org/10.1016/j.seppur.2005.04.007
Wang, Z., Fang, M., Yan, S., Yu, H., Wei, C.C., Luo, Z., 2013. Optimization of blended amines for CO2 absorption in a hollow-fiber membrane contactor. Ind. Eng. Chem. Res. https://doi.org/10.1021/ie401676t
Yan, S. ping, Fang, M.X., Zhang, W.F., Wang, S.Y., Xu, Z.K., Luo, Z.Y., Cen, K.F., 2007. Experimental study on the separation of CO2from flue gas using hollow fiber membrane contactors without wetting. Fuel Process. Technol. 88, 501–511. https://doi.org/10.1016/j.fuproc.2006.12.007
Yang, H., Xu, Z., Fan, M., Gupta, R., Slimane, R.B., Bland, A.E., Wright, I., 2008. Progress in carbon dioxide separation and capture: A review. J. Environ. Sci. https://doi.org/10.1016/S1001-0742(08)60002-9
Yeon, S.H., Lee, K.S., Sea, B., Park, Y.I., Lee, K.H., 2005. Application of pilot-scale membrane contactor hybrid system for removal of carbon dioxide from flue gas. J. Memb. Sci. 257, 156–160. https://doi.org/10.1016/j.memsci.2004.08.037
Yim, J.H., Ha, S.J., Lim, J.S., 2018. Measurement and Correlation of CO2Solubility in 1-Ethyl-3-methylimidazolium ([EMIM]) Cation-Based Ionic Liquids: [EMIM][Ac], [EMIM][Cl], and [EMIM][MeSO4]. J. Chem. Eng. Data 63, 508–518. https://doi.org/10.1021/acs.jced.7b00532
Ying, H., Baltus, R.E., 2007. Experimental measurement of the solubility and diffusivity of CO 2 in room-temperature ionic liquids using a transient thin-liquid-film method. Ind. Eng. Chem. Res. https://doi.org/10.1021/ie070501u
Yokozeki, A., Shiflett Mark, B., Junk Christopher, P., Grieco Liane, M., Foo, T., 2008. Physical and chemical absorptions of carbon dioxide in room-temperature ionic liquids. J. Phys. Chem. B 112, 16654–16663.
Zhang, H.Y., Wang, R., Liang, D.T., Tay, J.H., 2006. Modeling and experimental study of CO2absorption in a hollow fiber membrane contactor. J. Memb. Sci. 279, 301–310. https://doi.org/10.1016/j.memsci.2005.12.017
Zhang, Xiangping, Zhang, Xiaochun, Dong, H., Zhao, Z., Zhang, S., Huang, Y., 2012. Carbon capture with ionic liquids: overview and progress. Energy Environ. Sci. 5, 6668. https://doi.org/10.1039/c2ee21152a
Zhang, Y., Sunarso, J., Liu, S., Wang, R., 2013. Current status and development of membranes for CO2/CH4 separation: A review. Int. J. Greenh. Gas Control. https://doi.org/10.1016/j.ijggc.2012.10.009
Zhao, S., Cao, C., Wardhaugh, L., Feron, P.H.M., 2015a. Membrane evaporation of amine solution for energy saving

in post-combustion carbon capture: Performance evaluation. J. Memb. Sci. https://doi.org/10.1016/j.memsci.2014.09.029

Zhao, S., Feron, P.H.M., Cao, C., Wardhaugh, L., Yan, S., Gray, S., 2015b. Membrane evaporation of amine solution for energy saving in post-combustion carbon capture: Wetting and condensation. Sep. Purif. Technol. https://doi.org/10.1016/j.seppur.2015.03.015

Zhao, S., Feron, P.H.M., Deng, L., Favre, E., Chabanon, E., Yan, S., Hou, J., Chen, V., Qi, H., 2016. Status and progress of membrane contactors in post-combustion carbon capture: A state-of-the-art review of new developments. J. Memb. Sci. 511, 180–206. https://doi.org/10.1016/j.memsci.2016.03.051

Zubeir, L.F., Romanos, G.E., Weggemans, W.M.A., Iliev, B., Schubert, T.J.S., Kroon, M.C., 2015. Solubility and Diffusivity of CO<inf>2</inf> in the Ionic Liquid 1-Butyl-3-methylimidazolium Tricyanomethanide within a Large Pressure Range (0.01 MPa to 10 MPa). J. Chem. Eng. Data 60, 1544–1562. https://doi.org/10.1021/je500765m